J Geod (2009) 83:595–619
DOI 10.1007/s00190-008-0275-0

ORIGINAL ARTICLE

Methods of harmonic synthesis for global geopotential models and their first-, second- and third-order gradients

E. Fantino · S. Casotto

Received: 21 November 2006 / Accepted: 14 September 2008 / Published online: 5 November 2008

Abstract Four widely used algorithms for the computation of the Earth's gravitational potential and its first-, second- and third-order gradients are examined: the traditional increasing degree recursion in associated Legendre functions and its variant based on the Clenshaw summation, plus the methods of Pines and Cunningham–Metris, which are free from the singularities that distinguish the first two methods at the geographic poles. All four methods are reorganized with the lumped coefficients approach, which in the cases of Pines and Cunningham–Metris requires a complete revision of the algorithms. The characteristics of the four methods are studied and described, and numerical tests are performed to assess and compare their precision, accuracy, and efficiency. In general the performance levels of all four codes exhibit large improvements over previously published versions. From the point of view of numerical precision, away from the geographic poles Clenshaw and Legendre offer an overall better quality. Furthermore, Pines and Cunningham–Metris are affected by an intrinsic loss of precision at the equator and suffer from additional deterioration when the gravity gradients components are rotated into the East-North-Up topocentric reference system.

Keywords Geopotential · Spherical harmonics · Gravity tensors · Gravitational gradients · Associated Legendre functions · Helmholtz polynomials · Clenshaw summation

Electronic supplementary material The online version of this article (doi:10.1007/s00190-008-0275-0) contains supplementary material, which is available to authorized users.

E. Fantino · S. Casotto (✉)
Dipartimento di Astronomia, Università di Padova,
Vicolo dell'Osservatorio 3,
35122 Padua, Italy
e-mail: stefano.casotto@unipd.it

S. Casotto
Center for Space Studies (CISAS) "G. Colombo",
Università di Padova, Via Venezia 15,
35131 Padua, Italy

1 Introduction

The computation of the Earth's gravitational potential V and its gradients is fundamental to many applications in geodesy and geophysics. In particular, the second-order gradients of the geopotential are of interest to gravity field determination from satellite gravity gradiometry (SGG) and, more specifically, to the process of harmonic synthesis as part of the least squares accumulation phase in the estimation of the gravitational field coefficients. The simulation of the third derivatives may be useful in projecting the gravity gradients onto a reference sphere when performing the space-wise gridding of SGG data (Rummel and Colombo 1985; Tóth and Földváry 2005). Tóth (2005) models the time variation of the Eötvös tensor by expansion into Taylor series, linearly truncated at the third-order gradient. Higher-order derivatives may also be applied to approximate the acceleration difference by a Taylor expansion around the barycenter of a twin satellite configuration (Keller and Sharifi 2005).

The synthesis of the potential and its gradients becomes a task of major concern when dealing with large amounts of field points and high-resolution gravity models: this is the case of the satellite gravity gradiometry mission GOCE (Gravity Field and Steady-State Ocean Circulation Explorer) (Rummel et al. 1993; ESA 1999; Albertella et al. 2002; Drinkwater et al. 2003) in which $\approx 100 \times 10^6$ observation points are accumulated to determine $\approx 9 \times 10^4$ Stokes coefficients. In cases like this, aspects such as the numerical

accuracy and the computational performance of the algorithms adopted are issues of primary importance.

Many different representations of the gravitational potential of an extended body are available, but the most common appear to be those based on spherical harmonic (SH) functions. Alternative formulations include models in spheroidal harmonics (Heiskanen and Moritz 1967; Thông and Grafarend 1989) or ellipsoidal harmonics (Garmier and Barriot 2001), mass point or mass concentration (mascon) models (Sutton et al. 1991; Jackson et al. 1991; Michelson 1970; Konopliv et al. 1998), and finite element representations (Junkins 1976; Junkins and Engels 1979), but they will not be considered in this contribution.

SH formulations can be classified on the basis of the coordinates used in the representation of the field point and the character of the intervening special functions. The choice of the coordinates is closely connected to the presence of singularities in the representation. In fact, the use of spherical polar coordinates in the SH formulation of the potential leads to singularities of the gradients at the poles (Pines 1973; Lundberg and Schutz 1988; Koop and Stelpstra 1989; Balmino et al. 1990, 1991; Metris et al. 1999). On the other hand, if the SH functions are represented in Cartesian coordinates, these singularities disappear, as in the case of the Cunningham (1970) representation of the potential. Other important areas of concern in SH synthesis, as noted in Bettadpur et al. (1992), are the selection of the algorithms for the recursive computation of the associated Legendre functions (ALFs) (or their equivalents) and the issue of the arrangement of the computations for optimal performance (Koop and Stelpstra 1989; Holmes and Featherstone 2002a,b).

Some of these aspects have been investigated by several authors. Tscherning et al. (1983) tested four methods for the computation of various gravimetric quantities, only two of which are of direct interest to the present analysis; these methods were compared in terms of execution times for various sets of field points. Balmino et al. (1990) tested the performance and the accuracy of a variant of the *Pines* algorithm (see below) for the computation of the geopotential and its first- and second-order gradients. Balmino et al. (1991) presented comparisons of four software packages for the computation of the second-order gradient of the geopotential with the aim of estimating the computational capabilities and numerical accuracies of the process of harmonic synthesis within satellite gravity gradiometry. Metris et al. (1999) validated their extension of the *Cunningham* algorithm through comparison with Balmino et al. (1990) in terms of execution time and relative numerical agreement of various gravity gradient components, supplemented by internal checks on the cancellation of the Laplacian.

The results of these studies are still valid in several respects, but computer technology has improved considerably in the last decade to warrant a general reexamination of the subject. Current practise makes it now possible to test algorithms using quadruple precision at 128 bits on a desktop computer. Besides, with reference to the computational aspects of the data reduction procedures for space missions like GOCE, for which the numerical burden associated with spherical harmonic synthesis can be substantial, an up-to-date investigation on the performance of the various algorithms and their implementations may be of benefit.

This contribution deals with the computation of the gravity gradients for space applications. Its resolution domain is limited to a maximum degree and order of 360, which is largely within the range covered by on-going space missions (the GOCE mission will estimate the gravity field approximately up to degree and order 200, see Migliaccio et al. 2004, 2006; Pail et al. 2005, 2006).

The situation significantly changes when dealing with ground-based applications, for which high-resolution gravity data and models are required. This has led to the development of very high-resolution models, most noticeably the forthcoming release of the Earth Gravitational Model (EGM) complete to degree and order 2190 (Pavlis et al. 2005), and to the formulation of methods to overcome the numerical problems inherent in the synthesis of extended ranges of harmonic functions, i.e., the numerical underflow caused by the wide range of magnitudes that the Legendre functions assume as the latitude increases. Notable contributions to the solution of such problems are those by Holmes and Featherstone (2002a,b), who modified existing recursion algorithms for evaluating partial sums of ALFs and their first- and second-order derivatives up to high degree and order (e.g., up to 2700). More recently, Jekeli et al. (2007) formulated an operational approach to identify and neglect the numerically insignificant terms in spherical harmonic series up to degree 10,800, and thus avoid the numerical underflow and, at the same time, obtain considerable computational savings.

In the spherical harmonic range considered in this study (i.e., $n, m \leq 360$), some underflow of the spherical harmonic functions does occur, but its effect on the gravity gradients is absolutely negligible already in double floating-point precision.

This contribution is an investigation on four widely used methods for the computation of the gravitational potential and its first-, second- and third-order gradients:

- *Legendre*: the traditional increasing-degree recursion of the ALFs in local coordinates (see below);
- *Clenshaw*: a revision of the *Legendre* method based on the Clenshaw approach to the summation of products of coefficients times functions obeying a three-term recurrence relation;
- *Pines*: the method proposed by Pines (1973), based on derived Legendre polynomials in global coordinates (see

below) and here presented as an increasing-degree recursion algorithm;
– *Cunningham–Metris*: the method developed by Cunningham (1970) and extended by Metris et al. (1999), consisting in an increasing-degree recursion on a certain differential operator in global coordinates.

Pines and *Cunningham–Metris* are devoid of singularities at the geographic poles, a flaw that affects the gradients of the ALFs, and hence the algorithms of *Clenshaw* and *Legendre*. *Legendre* and *Clenshaw* are effectively two different arrangements of the same method.

In this work, the theoretical formulation of each method has been re-examined and in most cases largely, if not entirely, revised for better performance, as will be made clear in the exposition below. The gradients have been extended to the third order for each of the methods, except for *Cunningham–Metris*, which is already formulated for arbitrary order. Each algorithm has been formulated with the "lumped coefficients" approach (see below) and has been implemented in a dedicated software tool written in Fortran95. The software codes were tailored to single-processor, desktop computers. With the aim of providing coherent and homogeneous comparisons, each of these four methods has been run on a set of test cases and the results compared on the basis of performance, accuracy and precision.

The paper is organized as follows: Sect. 2 defines the two coordinate systems used in this work; then the development of each of the four algorithms is described in a dedicated section (Sects. 3–6); Sect. 7 illustrates the numerical tests adopted to assess numerical efficiency (Sect. 7.1), relative numerical precision (Sect. 7.2) and numerical accuracy (Sect. 7.3); the results of the comparisons are discussed in Sect. 8.

For the sake of brevity, references to Pines (1973), Cunningham (1970) and Metris et al. (1999) will be denoted PN73, CN70 and MT99, respectively.

2 Coordinate systems

The algorithms discussed here compute the gravity gradients with respect to either of two reference systems: the first system is used to specify the position of the observation point P, the second is naturally defined at P by the local gradient of position with respect to the spherical coordinates used to represent the potential. Both reference systems are fixed with the body and are shown in Fig. 1. They are more specifically defined as:

1. The global, bodycentric reference system $(O, \mathbf{i}_1, \mathbf{i}_2, \mathbf{i}_3)$: its origin O centred within the body, it is endowed with both a Cartesian coordinate system (O, x, y, z), and a spherical equatorial coordinate system (O, λ, φ, r). The basis vectors $\mathbf{i}_1, \mathbf{i}_2, \mathbf{i}_3$ form an orthonormal basis. The xy plane of this system defines the equatorial plane, the x-axis is oriented towards the fundamental meridian, the z-axis is aligned with the rotation axis of the body and points to the North geographic pole, the y-axis completing an orthogonal, right-handed triad. This is the reference system in which the geopotential coefficients are given. More on the relationships among the several reference frames used in space geodesy can be found in McCarthy and Petit (2004).
2. The local, or East-North-Up (ENU) topocentric reference system $(P, \mathbf{e}_1, \mathbf{e}_2, \mathbf{e}_3)$: its origin is at the field point P and the coordinate system associated with it is denoted by (P, ξ, η, ζ). The associated orthonormal basis $(\mathbf{e}_1, \mathbf{e}_2, \mathbf{e}_3)$ has the $\mathbf{e}_1$-axis oriented to the East, the $\mathbf{e}_2$-axis directed to the North and the $\mathbf{e}_3$-axis pointing radially outwards.

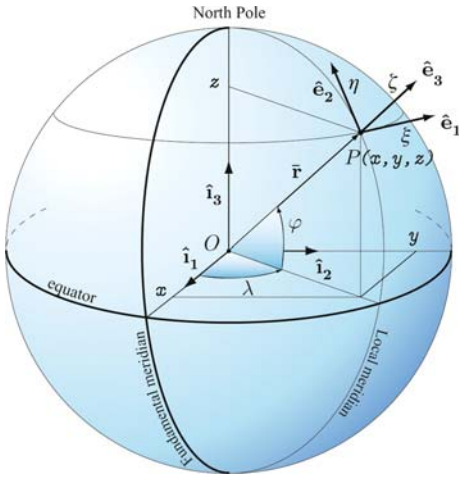

Fig. 1 The global reference system $(O, \mathbf{i}_1, \mathbf{i}_2, \mathbf{i}_3)$ and the local reference system $(P, \mathbf{e}_1, \mathbf{e}_2, \mathbf{e}_3)$

More on the relationships among the several reference frames used in space geodesy can be found in McCarthy and Petit (2004).

3 The method of Legendre

The conventional and traditional approach for expressing and evaluating the gravitational potential V at an external point P (i.e., outside the Brillouin sphere, Vanicek and Krakiwski 1986) by means of a spherical harmonic expansion in ALFs (Heiskanen and Moritz 1967) is

$$V(r, \varphi, \lambda) = \frac{GM}{r} \sum_{n=0}^{\infty} \left(\frac{a}{r}\right)^n \sum_{m=0}^{n} \overline{P}_n^m(\sin\varphi) \left(\overline{C}_{nm} \cos m\lambda + \overline{S}_{nm} \sin m\lambda\right), \quad (1)$$

where r, φ and λ are the spherical coordinates of P defined above, a is the mean Earth's radius, GM is the Earth's gravitational parameter (the product of the Universal gravitational constant and the mass of the Earth), the quantities $\overline{C}_{nm}$ and $\overline{S}_{nm}$ are the fully normalized Stokes coefficients and, finally, $\overline{P}_n^m(\sin\varphi)$ is the fully normalized ALF (fnALF) of the first kind of degree n and order m

$$\overline{P}_n^m(\varphi) = N_{nm}\left[\frac{\cos^m\varphi}{n!2^n}\frac{\mathrm{d}^{n+m}}{\mathrm{d}(\sin\varphi)^{n+m}}(\sin^2\varphi-1)^n\right] \tag{2}$$

(henceforth the dependence of $\overline{P}_n^m$ on $\sin\varphi$ will be written as $\overline{P}_n^m(\varphi)$, unless omitted), with the full normalization factor

$$N_{nm} = \sqrt{(2-\delta_{0m})(2n+1)\frac{(n-m)!}{(n+m)!}}, \tag{3}$$

where δ_{ij} is Kronecker's delta.

In practice, Eq. (1) is truncated at a maximum degree N which is related to the resolution of the gravity model.

The functions $\cos m\lambda$ and $\sin m\lambda$ are calculated through the recursions

$$\begin{aligned}\cos m\lambda &= \cos\lambda\cos(m-1)\lambda - \sin\lambda\sin(m-1)\lambda,\\ \sin m\lambda &= \cos\lambda\sin(m-1)\lambda + \sin\lambda\cos(m-1)\lambda,\end{aligned} \tag{4}$$

valid in the range $1 \le m \le N$.

As for the evaluation of the fnALFs and their derivatives, several methods are available. The ALFs satisfy numerous recurrence relations (tabulated for example in Abramowitz and Stegun 1964; Ilk 1983). There exist recurrences on n alone, on m alone, and on both n and m simultaneously; most recurrences having mixed strides are unstable and should be avoided (Bettadpur et al. 1992; Lundberg and Schutz 1988). Increasing-degree and decreasing-order recurrences for $P_n^m(\varphi)$ are known to be stable (Gautschi 1967).

The procedure adopted here to generate a set of fnALFs complete to degree and order N is the well-known increasing-degree recursion (IDR) (Hobson 1965), which is exhibited graphically in (Fig. 2). It consists in initializing $\overline{P}_0^0(\varphi) = 1$ and then computing the sectorial terms ($m = n$) by means of

$$\overline{P}_n^n(\varphi) = f_n\cos\varphi\,\overline{P}_{n-1}^{n-1}(\varphi), \quad n \ge 1, \tag{5}$$

with

$$f_n = \sqrt{\frac{(1+\delta_{1n})(2n+1)}{2n}}. \tag{6}$$

The remaining terms (zonals and tesserals: $0 \le m \le n-1$) are then obtained from the recursion

$$\overline{P}_n^m(\varphi) = g_{nm}\sin\varphi\,\overline{P}_{n-1}^m(\varphi) - h_{nm}\overline{P}_{n-2}^m(\varphi), \quad n \ge m+1 \tag{7}$$

where $\overline{P}_{n-1}^n(\varphi) = 0$ and

$$g_{nm} = \sqrt{\frac{(2n+1)(2n-1)}{(n+m)(n-m)}} \tag{8}$$

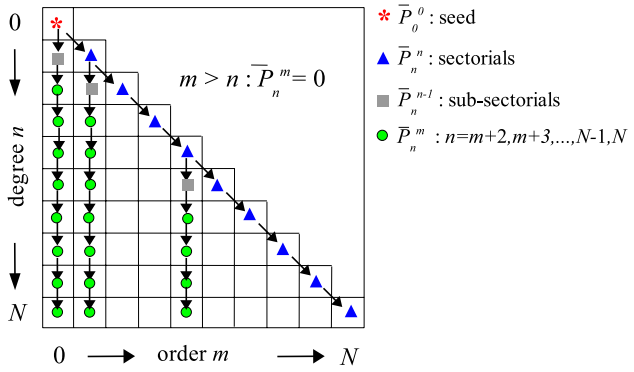

Fig. 2 Illustration of the IDR scheme for the evaluation of the (fn)ALFs. In the lower triangular part of the matrix each square corresponds to a specific combination of n and m: starting from the seed $\overline{P}_0^0$, all the diagonal terms are obtained, and from each of them the (fn)ALFs of constant m (*column*) are computed by sequentially increasing n (down and away from the diagonal)

and

$$h_{nm} = \frac{g_{nm}}{g_{n-1,m}} = \sqrt{\frac{(2n+1)(n-m-1)(n+m-1)}{(2n-3)(n+m)(n-m)}}, \tag{9}$$

while the remaining fnALFs with $m > n$ are defined to be zero.

The first derivatives of the fnALFs with respect to φ are given by (Robin 1957; Sansone 1991)

$$\frac{\mathrm{d}\overline{P}_n^m(\varphi)}{\mathrm{d}\varphi} = k_{nm}\overline{P}_n^{m+1}(\varphi) - m\tan\varphi\,\overline{P}_n^m(\varphi), \tag{10}$$

where

$$k_{nm} = \sqrt{\frac{(2-\delta_{o,m})(n-m)(n+m+1)}{2}}. \tag{11}$$

The second-order derivative can be directly obtained from Legendre's differential equation (Heiskanen and Moritz 1967):

$$\begin{aligned}\frac{\mathrm{d}^2\overline{P}_n^m(\varphi)}{\mathrm{d}\varphi^2} &= \left[m^2\sec^2\varphi - n(n+1)\right]\overline{P}_n^m(\varphi)\\ &\quad + \tan\varphi\frac{\mathrm{d}\overline{P}_n^m(\varphi)}{\mathrm{d}\varphi}.\end{aligned} \tag{12}$$

Differentiation of Eq. (12) provides the third-order derivative of the fnALF,

$$\begin{aligned}\frac{\mathrm{d}^3\overline{P}_n^m(\varphi)}{\mathrm{d}\varphi^3} &= 2m^2\tan\varphi\sec^2\varphi\,\overline{P}_n^m(\varphi) + \tan\varphi\frac{\mathrm{d}^2\overline{P}_n^m(\varphi)}{\mathrm{d}\varphi^2}\\ &\quad + \left[(m^2+1)\sec^2\varphi - n(n+1)\right]\frac{\mathrm{d}\overline{P}_n^m(\varphi)}{\mathrm{d}\varphi}.\end{aligned} \tag{13}$$

At the geographic poles (where $\varphi = \pm\pi/2$), the $\tan\varphi$ and $\sec^2\varphi$ terms in Eqs. (10), (12) and (13) cause singularities in the derivatives of the fnALFs.

Table 1 The first-order partial derivatives of the geopotential in the *Legendre* algorithm

$$V_\lambda = -\frac{GM}{r}\sum_{m=0}^{N} m\left(A_m^{(0)}\sin\lambda - B_m^{(0)}\cos\lambda\right)$$
$$V_\varphi = \frac{GM}{r}\sum_{m=0}^{N}\left(A_m^{(\varphi)}\cos\lambda + B_m^{(\varphi)}\sin\lambda\right)$$
$$V_r = -\frac{GM}{r^2}\sum_{m=0}^{N}\left(A_m^{(r)}\cos\lambda + B_m^{(r)}\sin\lambda\right)$$

3.1 Lumped coefficients synthesis of the geopotential and its gradients

For computational reasons it is often convenient (e.g., when the observation points are located at the nodes of a regular, spherical grid) to invert the summations over n and m that appear in Eq. (1) to obtain

$$V = \frac{GM}{r}\sum_{m=0}^{N}\left(A_m^{(0)}\cos m\lambda + B_m^{(0)}\sin m\lambda\right), \tag{14}$$

with the so-called "lumped coefficients" $A_m^{(0)}$ and $B_m^{(0)}$ given by

$$A_m^{(0)} = \sum_{n=m}^{N}\left(\frac{a}{r}\right)^n \overline{C}_{nm}\overline{P}_n^m(\varphi), \tag{15}$$

$$B_m^{(0)} = \sum_{n=m}^{N}\left(\frac{a}{r}\right)^n \overline{S}_{nm}\overline{P}_n^m(\varphi). \tag{16}$$

The first-, second- and third-order partial derivatives of V can be expressed in lumped-coefficient forms similar to that of the potential, Eqs. (14), (15) and (16). They are exhibited in Tables 1, 2 and 3, with the associated lumped coefficients provided separately in Tables 4, 5 and 6. The physical components of the gravity gradients can then be computed using the expressions given, e.g., in Tables 2, 3, and 4 of Casotto and Fantino (2008). Other references dealing with the first- and second-order gravity gradient components are, e.g., Long et al. (1989); Eddy et al. (1990); Vallado (2001); Xu (2003).

4 The method of Clenshaw

The algorithm developed by Clenshaw (1955) and known under the name of *Clenshaw summation* algorithm is a rearrangement of the *Legendre* method based on the Clenshaw approach to the summation of coefficients times functions obeying a three-term recurrence relation. It was originally introduced as a recursion method to evaluate summations of series of Chebyshev polynomials without rearranging them in power series (Clenshaw 1955), and was adapted to the case of ALFs by Tscherning (1976).

A general description of the algorithm can be found in Appendix A (see also Press et al. 1992); its application to geodetic problems is discussed by Tscherning (1976) and Tscherning and Poder (1982); some of the numerical properties of the *Clenshaw* algorithm are studied by Smoktunowicz (2002) and references therein. Here we describe the application to the computation of the geopotential V and its gradients of the first, second and third order at an external point P. In this context, the Clenshaw summation method is intrinsically a lumped coefficients approach. It starts, e.g., with the geopotential V in the form of Eq. (14), which it will be expedient to rewrite in the form of Appendix A as

$$V = \frac{GM}{r}\sum_{m=0}^{N}\left(v_m^{(1)}\cos m\lambda + v_m^{(2)}\sin m\lambda\right), \tag{17}$$

with the lumped coefficients $v_m^{(1)}$ and $v_m^{(2)}$ defined as

$$v_m^{(1)} = A_m^{(0)}, \tag{18}$$
$$v_m^{(2)} = B_m^{(0)}. \tag{19}$$

As in Eq. (A1), we write

$$v_m^{(i)} = \sum_{n=m}^{N} c_n^{(i)}\,\overline{p}_n, \quad i = 1, 2, \tag{20}$$

where

$$\overline{p}_n = \left(\frac{a}{r}\right)^n \overline{P}_n^m(\varphi) \tag{21}$$

and

$$c_n^{(i)} = \begin{cases} \overline{C}_{nm} & \text{for } i = 1, \\ \overline{S}_{nm} & \text{for } i = 2. \end{cases} \tag{22}$$

Table 2 The second-order partial derivatives of the geopotential in the *Legendre* algorithm

$$V_{\lambda\lambda} = -\frac{GM}{r}\sum_{m=0}^{N} m^2\left(A_m^{(0)}\cos\lambda + B_m^{(0)}\sin\lambda\right)$$
$$V_{\lambda\varphi} = \frac{GM}{r}\sum_{m=0}^{N} m\left(A_m^{(\varphi)}\sin\lambda - B_m^{(\varphi)}\cos\lambda\right)$$
$$V_{\lambda r} = \frac{GM}{r^2}\sum_{m=0}^{N} m\left(A_m^{(r)}\sin\lambda - B_m^{(r)}\cos\lambda\right)$$
$$V_{\varphi\varphi} = \frac{GM}{r}\sum_{m=0}^{N}\left(A_m^{(\varphi\varphi)}\cos\lambda + B_m^{(\varphi\varphi)}\sin\lambda\right)$$
$$V_{\varphi r} = -\frac{GM}{r^2}\sum_{m=0}^{N}\left(A_m^{(\varphi r)}\cos\lambda + B_m^{(\varphi r)}\sin\lambda\right)$$
$$V_{rr} = \frac{GM}{r^3}\sum_{m=0}^{N}\left(A_m^{(rr)}\cos\lambda + B_m^{(rr)}\sin\lambda\right)$$

Table 3 The third-order partial derivatives of the geopotential in the *Legendre* algorithm

$$V_{\lambda\lambda\lambda} = \frac{GM}{r}\sum_{m=0}^{N} m^3\left(A_m^{(0)}\sin\lambda - B_m^{(0)}\cos\lambda\right) \qquad V_{\lambda\lambda\varphi} = -\frac{GM}{r}\sum_{m=0}^{N} m^2\left(A_m^{(\varphi)}\cos\lambda + B_m^{(\varphi)}\sin\lambda\right)$$
$$V_{\lambda\lambda r} = \frac{GM}{r^2}\sum_{m=0}^{N} m^2\left(A_m^{(r)}\cos\lambda + B_m^{(r)}\sin\lambda\right) \qquad V_{\varphi\varphi\lambda} = -\frac{GM}{r}\sum_{m=0}^{N} m\left(A_m^{(\varphi\varphi)}\sin\lambda - B_m^{(\varphi\varphi)}\cos\lambda\right)$$
$$V_{\varphi\varphi\varphi} = \frac{GM}{r}\sum_{m=0}^{N}\left(A_m^{(\varphi\varphi\varphi)}\cos\lambda + B_m^{(\varphi\varphi\varphi)}\sin\lambda\right) \qquad V_{\varphi\varphi r} = \frac{GM}{r^2}\sum_{m=0}^{N}\left(A_m^{(\varphi\varphi r)}\cos\lambda + B_m^{(\varphi\varphi r)}\sin\lambda\right)$$
$$V_{rr\lambda} = -\frac{GM}{r^3}\sum_{m=0}^{N} m\left(A_m^{(rr)}\sin\lambda - B_m^{(rr)}\cos\lambda\right) \qquad V_{rr\varphi} = \frac{GM}{r^3}\sum_{m=0}^{N}\left(A_m^{(rr\varphi)}\cos\lambda + B_m^{(rr\varphi)}\sin\lambda\right)$$
$$V_{rrr} = \frac{GM}{r^4}\sum_{m=0}^{N}\left(A_m^{(rrr)}\cos\lambda + B_m^{(rrr)}\sin\lambda\right) \qquad V_{\lambda\varphi r} = \frac{GM}{r^2}\sum_{m=0}^{N} m\left(A_m^{(\varphi r)}\sin\lambda - B_m^{(\varphi r)}\cos\lambda\right)$$

Table 4 The lumped coefficients for the first-order partial derivatives of the geopotential in the *Legendre* method

$$A_m^{(\varphi)} = \sum_{n=m}^{N}\left(\frac{a}{r}\right)^n \overline{C}_{nm}\frac{\mathrm{d}\overline{P}_n^m}{d\varphi} \qquad B_m^{(\varphi)} = \sum_{n=m}^{N}\left(\frac{a}{r}\right)^n \overline{S}_{nm}\frac{\mathrm{d}\overline{P}_n^m}{d\varphi}$$
$$A_m^{(r)} = \sum_{n=m}^{N}\left(\frac{a}{r}\right)^n (n+1)\overline{C}_{nm}\overline{P}_n^m \qquad B_m^{(r)} = \sum_{n=m}^{N}\left(\frac{a}{r}\right)^n (n+1)\overline{S}_{nm}\overline{P}_n^m$$

For the sake of brevity, since the order m is fixed, the corresponding subscript does not appear in the p_n functions and in the $c_n^{(i)}$ coefficients.

Now consider the recursion formula in Eq. (7) for normalized tesseral and zonal fnALFs

$$\overline{P}_n^m(u) = u g_{nm}\overline{P}_{n-1}^m(u) - h_{nm}\overline{P}_{n-2}^m(u), \tag{23}$$

with $0 \le m \le n-1$, $n = 1, 2, \ldots, N$, and

$$u = \sin\varphi. \tag{24}$$

After multiplication of each side by q^n, where

$$q = a/r, \tag{25}$$

we obtain

$$q^n\overline{P}_n^m = u g_{nm} q q^{n-1}\overline{P}_{n-1}^m - h_{nm} q^2 q^{n-2}\overline{P}_{n-2}^m. \tag{26}$$

With the notation of Eq. (A2), Eq. (26) becomes

$$\overline{p}_n - \alpha_{nm}\overline{p}_{n-1} + \beta_{nm}\overline{p}_{n-2} = 0 \tag{27}$$

initialized by $\overline{p}_1 = \alpha_1$ and $\overline{p}_0 = 1$, the coefficients α_n and β_n being defined as

$$\begin{aligned}\alpha_n &= u q g_{nm}\\ \beta_n &= q^2 h_{nm},\end{aligned} \tag{28}$$

Table 5 The lumped coefficients of the second-order partial derivatives of the geopotential in the *Legendre* algorithm

$$A_m^{(\varphi\varphi)} = \sum_{n=m}^{N}\left(\frac{a}{r}\right)^n \overline{C}_{nm}\frac{\mathrm{d}^2\overline{P}_n^m}{d\varphi^2} \qquad B_m^{(\varphi\varphi)} = \sum_{n=m}^{N}\left(\frac{a}{r}\right)^n \overline{S}_{nm}\frac{\mathrm{d}^2\overline{P}_n^m}{d\varphi^2}$$
$$A_m^{(\varphi r)} = \sum_{n=m}^{N}\left(\frac{a}{r}\right)^n (n+1)\overline{C}_{nm}\frac{\mathrm{d}\overline{P}_n^m}{d\varphi} \qquad B_m^{(\varphi r)} = \sum_{n=m}^{N}\left(\frac{a}{r}\right)^n (n+1)\overline{S}_{nm}\frac{\mathrm{d}\overline{P}_n^m}{d\varphi}$$
$$A_m^{(rr)} = \sum_{n=m}^{N}\left(\frac{a}{r}\right)^n (n+1)(n+2)\overline{P}_n^m \qquad B_m^{(rr)} = \sum_{n=m}^{N}\left(\frac{a}{r}\right)^n (n+1)(n+2)\overline{S}_{nm}\overline{P}_n^m$$

Table 6 The lumped coefficients of the third-order partial derivatives of the geopotential in the *Legendre* algorithm

$$A_m^{(\varphi\varphi\varphi)} = \sum_{n=m}^{N}\left(\frac{a}{r}\right)^n \overline{C}_{nm}\frac{\mathrm{d}^3\overline{P}_n^m}{d\varphi^3} \qquad B_m^{(\varphi\varphi\varphi)} = \sum_{n=m}^{N}\left(\frac{a}{r}\right)^n \overline{S}_{nm}\frac{\mathrm{d}^3\overline{P}_n^m}{d\varphi^3}$$
$$A_m^{(\varphi\varphi r)} = \sum_{n=m}^{N}\left(\frac{a}{r}\right)^n (n+1)\overline{C}_{nm}\frac{\mathrm{d}^2\overline{P}_n^m}{d\varphi^2} \qquad B_m^{(\varphi\varphi r)} = \sum_{n=m}^{N}\left(\frac{a}{r}\right)^n (n+1)\overline{S}_{nm}\frac{\mathrm{d}^2\overline{P}_n^m}{d\varphi^2}$$
$$A_m^{(rr\varphi)} = \sum_{n=m}^{N}\left(\frac{a}{r}\right)^n (n+1)(n+2)\overline{C}_{nm}\frac{\mathrm{d}\overline{P}_n^m}{d\varphi} \qquad B_m^{(rr\varphi)} = \sum_{n=m}^{N}\left(\frac{a}{r}\right)^n (n+1)(n+2)\overline{S}_{nm}\frac{\mathrm{d}\overline{P}_n^m}{d\varphi}$$
$$A_m^{(rrr)} = \sum_{n=m}^{N}\left(\frac{a}{r}\right)^n (n+1)(n+2)(n+3)\overline{P}_n^m \qquad B_m^{(rrr)} = \sum_{n=m}^{N}\left(\frac{a}{r}\right)^n (n+1)(n+2)(n+3)\overline{S}_{nm}\overline{P}_n^m$$

once again ignoring the dependence on the order m. Eq. (27) is the three-term recurrence relation required for the application of the *Clenshaw summation* algorithm to the summation of Eq. (20). Hence, according to Appendix A, for each $i = 1, 2$ there exists a set of $y_n^{(i)}$ coefficients such that

$$\begin{aligned}
y_{N+2}^{(i)} &= 0 \\
y_{N+1}^{(i)} &= 0 \\
y_N^{(i)} &= c_N^{(i)} \\
y_{N-1}^{(i)} &= c_{N-1}^{(i)} + \alpha_N y_N^{(i)} \\
&\cdots \\
y_k^{(i)} &= c_k^{(i)} + \alpha_{k+1} y_{k+1}^{(i)} - \beta_{k+2} y_{k+2}^{(i)} \\
y_{k-1}^{(i)} &= c_{k-1}^{(i)} + \alpha_k y_k^{(i)} - \beta_{k+1} y_{k+1}^{(i)} \\
&\cdots \\
y_m^{(i)} &= c_m^{(i)} + \alpha_{m+1} y_{m+1}^{(i)} - \beta_{m+2} y_{m+2}^{(i)}.
\end{aligned} \tag{29}$$

which covers all the degrees of interest (i.e., $m \le n \le N+2$). From Eq. (A7), we have

$$v_m^{(i)} = y_m^{(i)} \overline{p}_m + y_{m+1}^{(i)} \left(\overline{p}_{m+1} - \alpha_{m+1} \overline{p}_m \right) \tag{30}$$

which, after the substitution

$$\overline{p}_{m+1} - \alpha_{m+1} \overline{p}_m = -b_{m+1} \overline{p}_{m-1}, \tag{31}$$

yields

$$v_m^{(i)} = y_m^{(i)} \overline{p}_m - b_{m+1} y_{m+1}^{(i)} \overline{p}_{m-1}. \tag{32}$$

Since $\overline{p}_{m-1} = \overline{P}_{m-1}^m \equiv 0$, we finally obtain

$$v_m^{(i)} = y_m^{(i)} \overline{p}_m, \quad i = 1, 2. \tag{33}$$

The evaluation of Eq. (17) thus reduces to

$$V = \frac{GM}{r} \sum_{m=0}^{N} \left(y_m^{(1)} \cos m\lambda + y_m^{(2)} \sin m\lambda \right) \overline{p}_m. \tag{34}$$

Equation (34) shows that only the sectorials $\overline{p}_m$ need to be computed and stored. This is achieved by multiplying Eq. (5) by q^m for $n = m$, yielding

$$q^m \overline{P}_m^m(u) = f_m \sqrt{1-u^2}\, q\, q^{m-1} \overline{P}_{m-1}^{m-1}(u), \tag{35}$$

or

$$\overline{p}_m = f_m \sqrt{1-u^2}\, q\, \overline{p}_{m-1}, \tag{36}$$

in terms of the new functions $\overline{p}_m$. The coefficients f_m are defined in Eq. (6) and the starting value of the recursion on the $\overline{p}_m$ functions is $\overline{p}_0 = 1$.

4.1 Computation of the gravity gradients

The partial derivatives of any order of the gravitational potential V with respect to the local spherical coordinates λ, φ and r at the observation point P can be represented in a form similar to Eq. (34). Tscherning and Poder (1982) derive the explicit formulation of the first- and second-order derivatives of V. Tscherning (1976) discusses the derivatives of any order of the normal potential with respect to co-latitude and radial distance.

Here, we provide a description of the gradients complete to the third order ($\max(j+k+l) = 3$), which can be generally put in the form

$$D_{jkl} V = \sum_{w=0}^{k} \Xi_w(\varphi, r) \sum_{m=0}^{N} \left(v_{m,u^w r^l}^{(1)} - \mathrm{i} v_{m,u^w r^l}^{(2)} \right) \partial_{\lambda^j} e^{\mathrm{i}m\lambda} \tag{37}$$

where $D_{jkl} V$ indicates the partial derivative of V with respect to combinations of λ, φ and r that are severally required to compute the natural components of the gradients (Table 7),

$$D_{jkl} V \equiv \frac{\partial V}{\partial \lambda^j \partial \varphi^k \partial r^l}. \tag{38}$$

The functions $\Xi_w(\varphi, r)$ can be obtained by inspection of the various functions that appear as factors outside the summations in the gradient components of Table 7, including the various powers of $\cos\varphi$ and $\sin\varphi$ originating from the differentiation of u with respect to φ. The upper limit k of the summation on w depends on the specific gradient component and can vary from zero to three. The functions $v_{m,u^w r^l}^{(i)}$ are obtained by differentiation of Eq. (33) with respect to the corresponding combination of u and r. As shown in Table 9, their computation requires the sectorials $\overline{p}_m$ (Eq. 36) and their derivatives $\mathrm{d}\overline{p}_m/\mathrm{d}u$, $\mathrm{d}^2\overline{p}_m/\mathrm{d}u^2$ and $\mathrm{d}^3\overline{p}_m/\mathrm{d}u^3$. The latter can be obtained from Eq. (10) and its derivatives of first and second order, respectively:

$$\frac{\mathrm{d}\overline{p}_m}{\mathrm{d}u} = \left[(1-u^2) \frac{\mathrm{d}\overline{p}_{m-1}}{\mathrm{d}u} - u \overline{p}_{m-1} \right] \frac{q f_m}{(1-u^2)^{1/2}}, \tag{39}$$

$$\begin{aligned}
\frac{\mathrm{d}^2\overline{p}_m}{\mathrm{d}u^2} = \Bigg[& (1-u^2)^2 \frac{\mathrm{d}^2\overline{p}_{m-1}}{\mathrm{d}u^2} - 2u(1-u^2) \frac{\mathrm{d}\overline{p}_{m-1}}{\mathrm{d}u} \\
& - \overline{p}_{m-1} \Bigg] \frac{q f_m}{(1-u^2)^{3/2}},
\end{aligned} \tag{40}$$

$$\begin{aligned}
\frac{\mathrm{d}^3\overline{p}_m}{\mathrm{d}u^3} = \Bigg[& (1-u^2)^3 \frac{\mathrm{d}^3\overline{p}_{m-1}}{\mathrm{d}u^3} - 3u(1-u^2)^2 \frac{\mathrm{d}^2\overline{p}_{m-1}}{\mathrm{d}u^2} \\
& - 3(1-u^2) \frac{\mathrm{d}\overline{p}_{m-1}}{\mathrm{d}u} - 3u \overline{p}_{m-1} \Bigg] \frac{q f_m}{(1-u^2)^{5/2}}.
\end{aligned} \tag{41}$$

Finally, as in Eq. (32), the functions $v_{m,jkl}^{(i)}$ are related to the coefficients $y_{m,jkl}^{(i)}$, and these are computed through the three-term recursions of Table 8.

Table 7 The geopotential V and its partial derivatives of the first, second and third order with respect to λ, φ and r, in a form suitable for computation by the Clenshaw (1955) summation algorithm

$$V = \frac{GM}{r}\sum_{m=0}^{N}\left(v_m^{(1)}\cos m\lambda + v_m^{(2)}\sin m\lambda\right)$$

$$\partial_\varphi V = \frac{GM\cos\varphi}{r}\sum_{m=0}^{N}\left(v_{m,u}^{(1)}\cos m\lambda + v_{m,u}^{(2)}\sin m\lambda\right)$$

$$\partial_{\lambda\lambda} V = -\frac{GM}{r}\sum_{m=0}^{N} m^2(v_m^{(1)}\cos m\lambda + v_m^{(2)}\sin m\lambda)$$

$$\partial_{\varphi\varphi} V = \frac{GM\cos^2\varphi}{r}\sum_{m=0}^{N}\left(v_{m,uu}^{(1)}\cos m\lambda + v_{m,uu}^{(2)}\sin m\lambda\right) - \frac{GM\sin\varphi}{r}\sum_{m=0}^{N}\left(v_{m,u}^{(1)}\cos m\lambda + v_{m,u}^{(2)}\sin m\lambda\right)$$

$$\partial_{rr} V = \frac{GM}{r^3}\sum_{m=0}^{N}\left(v_{m,rr}^{(1)}\cos m\lambda + v_{m,rr}^{(2)}\sin m\lambda\right)$$

$$\partial_{\lambda\lambda\varphi} V = -\frac{GM\cos\varphi}{r}\sum_{m=0}^{N} m^2\left(v_{m,u}^{(1)}\cos m\lambda + v_{m,u}^{(2)}\sin m\lambda\right)$$

$$\partial_{\varphi\varphi\lambda} V = -\frac{GM\cos^2\varphi}{r}\sum_{m=0}^{N} m\left(v_{m,uu}^{(1)}\sin m\lambda - v_{m,uu}^{(2)}\cos m\lambda\right) + \frac{GM\sin\varphi}{r}\sum_{m=0}^{N} m\left(v_{m,u}^{(1)}\sin m\lambda - v_{m,u}^{(2)}\cos m\lambda\right)$$

$$\partial_{\varphi\varphi r} V = -\frac{GM\cos^2\varphi}{r^2}\sum_{m=0}^{N}\left(v_{m,uur}^{(1)}\cos m\lambda + v_{m,uur}^{(2)}\sin m\lambda\right) + \frac{GM\sin\varphi}{r^2}\sum_{m=0}^{N}\left(v_{m,ur}^{(1)}\cos m\lambda + v_{m,ur}^{(2)}\sin m\lambda\right)$$

$$\partial_{rr\varphi} V = \frac{GM\cos\varphi}{r^3}\sum_{m=0}^{N}\left(v_{m,urr}^{(1)}\cos m\lambda + v_{m,urr}^{(2)}\sin m\lambda\right)$$

$$\partial_{\lambda\varphi r} V = \frac{GM\cos\varphi}{r^2}\sum_{m=0}^{N} m\left(v_{m,ur}^{(1)}\sin m\lambda - v_{m,ur}^{(2)}\cos m\lambda\right)$$

$$\partial_\lambda V = -\frac{GM}{r}\sum_{m=0}^{N} m(v_m^{(1)}\sin m\lambda - v_m^{(2)}\cos m\lambda)$$

$$\partial_r V = -\frac{GM}{r^2}\sum_{m=0}^{N}\left(v_{m,r}^{(1)}\cos m\lambda + v_{m,r}^{(2)}\sin m\lambda\right)$$

$$\partial_{\lambda\varphi} V = -\frac{GM\cos\varphi}{r}\sum_{m=0}^{N} m\left(v_{m,u}^{(1)}\sin m\lambda - v_{m,u}^{(2)}\cos m\lambda\right)$$

$$\partial_{\lambda r} V = \frac{GM}{r^2}\sum_{m=0}^{N} m\left(v_{m,r}^{(1)}\sin m\lambda - v_{m,r}^{(2)}\cos m\lambda\right)$$

$$\partial_{\varphi r} V = -\frac{GM\cos\varphi}{r^2}\sum_{m=0}^{N}\left(v_{m,ur}^{(1)}\cos m\lambda + v_{m,ur}^{(2)}\sin m\lambda\right)$$

$$\partial_{\lambda\lambda\lambda} V = \frac{GM}{r}\sum_{m=0}^{N} m^3(v_m^{(1)}\sin m\lambda - v_m^{(2)}\cos m\lambda)$$

$$\partial_{\lambda\lambda r} V = \frac{GM}{r^2}\sum_{m=0}^{N} m^2\left(v_{m,r}^{(1)}\cos m\lambda + v_{m,r}^{(2)}\sin m\lambda\right)$$

$$\partial_{\varphi\varphi\varphi} V = \frac{GM\cos^3\varphi}{r}\sum_{m=0}^{N}\left(v_{m,uuu}^{(1)}\cos m\lambda + v_{m,uuu}^{(2)}\sin m\lambda\right) - \frac{3GM\sin\varphi\cos\varphi}{r}\sum_{m=0}^{N}\left(v_{m,uu}^{(1)}\cos m\lambda + v_{m,uu}^{(2)}\sin m\lambda\right) - \frac{GM\cos\varphi}{r}\sum_{m=0}^{N}\left(v_{m,u}^{(1)}\cos m\lambda + v_{m,u}^{(2)}\sin m\lambda\right)$$

$$\partial_{rr\lambda} V = -\frac{GM}{r^3}\sum_{m=0}^{N} m\left(v_{m,rr}^{(1)}\sin m\lambda - v_{m,rr}^{(2)}\cos m\lambda\right)$$

$$\partial_{rrr} V = -\frac{GM}{r^4}\sum_{m=0}^{N}\left(v_{m,rrr}^{(1)}\cos m\lambda + v_{m,rrr}^{(2)}\sin m\lambda\right)$$

Table 8 *Clenshaw* method: seeds (second, third and fourth column) and general three-term recursion (fifth column) for each set of $y_{n,jkl}^{(i)}$ coefficients

jkl	$y_{N+2,jkl}^{(i)}$	$y_{N+1,jkl}^{(i)}$	$y_{N,jkl}^{(i)}$	$y_{n,jkl}^{(i)} =$
–	0	0	$c_N^{(i)}$	$c_n^{(i)} + uqg_{n+1,m}y_{n+1}^{(i)} - q^2h_{n+2,m}y_{n+2}^{(i)}$
r	0	0	$c_N^{(i)}(N+1)$	$c_n^{(i)}(n+1) + uqg_{n+1,m}y_{n+1,r}^{(i)} - q^2h_{n+2,m}y_{n+2,r}^{(i)}$
u	0	0	0	$uqg_{n+1,m}y_{n+1,u}^{(i)} + qg_{n+1,m}y_{n+1}^{(i)} - q^2h_{n+2,m}y_{n+2,u}^{(i)}$
uu	0	0	0	$2qg_{n+1,m}y_{n+1,u}^{(i)} + uqg_{n+1,m}y_{n+1,uu}^{(i)} - q^2h_{n+2,m}y_{n+2,uu}^{(i)}$
ur	0	0	0	$qg_{n+1,m}y_{n+1,r}^{(i)} + uqg_{n+1,m}y_{n+1,ur}^{(i)} - q^2h_{n+2,m}y_{n+2,ur}^{(i)}$
rr	0	0	$c_N^{(i)}(N+1)(N+2)$	$c_n^{(i)}(n+1)(n+2) + uqg_{n+1,m}y_{n+1,rr}^{(i)} - q^2h_{n+2,m}y_{n+2,rr}^{(i)}$
uuu	0	0	0	$3qg_{n+1,m}y_{n+1,uu}^{(i)} + uqg_{n+1,m}y_{n+1,uuu}^{(i)} - q^2h_{n+2,m}y_{n+2,uuu}^{(i)}$
uur	0	0	0	$uqg_{n+1,m}y_{n+1,uur}^{(i)} + 2qg_{n+1,m}y_{n+1,ur}^{(i)} - q^2h_{n+2,m}y_{n+2,uur}^{(i)}$
urr	0	0	0	$uqg_{n+1,m}y_{n+1,urr}^{(i)} + qg_{n+1,m}y_{n+1,rr}^{(i)} - q^2h_{n+2,m}y_{n+2,urr}^{(i)}$
rrr	0	0	$c_N^{(i)}(N+1)(N+2)(N+3)$	$c_n^{(i)}(n+1)(n+2)(n+3) + uqg_{n+1,m}y_{n+1,rrr}^{(i)} - q^2h_{n+2,m}y_{n+2,rrr}^{(i)}$

The subscript jkl (first column) indicates the combination of variables with respect to which the specific geopotential derivative is made

Table 9 Definition of the $v^{(i)}_{m,jkl}$ terms used in the *Clenshaw* method for computing the partial derivatives of first, second and third order of the geopotential

$$
\begin{aligned}
v^{(i)}_{m} &= y^{(i)}_{m}\, p_m \\
v^{(i)}_{m,u} &= y^{(i)}_{m}\frac{dp_m}{du} + y^{(i)}_{m,u}\, p_m \\
v^{(i)}_{m,r} &= y^{(i)}_{m,r}\, p_m \\
v^{(i)}_{m,uu} &= y^{(i)}_{m,uu}\, p_m + \frac{\mathrm{d}^2 p_m}{du^2} y^{(i)}_{m} + 2y^{(i)}_{m,u}\frac{dp_m}{du} \\
v^{(i)}_{m,ur} &= y^{(1)}_{m,r}\frac{dp_m}{du} + y^{(1)}_{m,ur}\, p_m \\
v^{(i)}_{m,rr} &= y^{(i)}_{m,rr}\, p_m \\
v^{(i)}_{m,uuu} &= y^{(i)}_{m,uuu}\, p_m + \frac{\mathrm{d}^3 p_m}{du^3} y^{(i)}_{m} + 3y^{(i)}_{m,uu}\frac{dp_m}{du} + 3y^{(i)}_{m,u}\frac{\mathrm{d}^2 p_m}{du^2} \\
v^{(i)}_{m,uur} &= y^{(i)}_{m,uur}\, p_m + \frac{\mathrm{d}^2 p_m}{du^2} y^{(i)}_{m,r} + 2y^{(i)}_{m,ur}\frac{dp_m}{du} \\
v^{(i)}_{m,urr} &= y^{(i)}_{m,rr}\frac{dp_m}{du} + y^{(i)}_{m,urr}\, p_m \\
v^{(i)}_{m,rrr} &= y^{(i)}_{m,rrr}\, p_m
\end{aligned}
$$

The subscript jkl indicates the combination of variables with respect to which the specific geopotential derivative is made

5 The method of Pines

In PN73 the geopotential and its first- and second-order gradients are represented in terms of so-called "derived Legendre polynomials" (Lundberg and Schutz 1988) or "Helmholtz polynomials" (HPs) (Balmino et al. 1990, 1991) in the global reference system. The value of the method is that it naturally provides a singularity-free representation of the gradients.

In PN73, the x, y, z Cartesian coordinates of the field point P are replaced by the direction cosines s, t and u of the position of P

$$
\begin{aligned}
s &= x/r = \cos\varphi\cos\lambda, \\
t &= y/r = \cos\varphi\sin\lambda, \\
u &= z/r = \sin\varphi,
\end{aligned}
\tag{42}
$$

and supplemented by the radial distance r from the centre as a fourth variable, thus making the set redundant. The ALFs are replaced by HPs H^m_n

$$
H^m_n(u) = \frac{1}{n!2^n}\frac{\mathrm{d}^{n+m}}{\mathrm{d}u^{n+m}}(u^2-1)^n. \tag{43}
$$

The Earth's gravitational potential V at P can then be written as the following series expansion (truncated at a maximum degree N):

$$
V(P) = V(s,t,u,r) = \sum_{n=0}^{N}\rho_n\sum_{m=0}^{n} D_{nm}(s,t)H^m_n(u), \tag{44}
$$

where the parallactic factor $\rho_n = GM/r\,(a/r)^n$ is computed recursively through

$$
\rho_n = \left(\frac{a}{r}\right)\rho_{n-1}, \quad \rho_0 = \frac{GM}{r}, \quad n = 1,2,\ldots,N, \tag{45}
$$

and $D_{nm}(s,t)$ is called the "mass coefficient function" of degree n and order m

$$
D_{nm}(s,t) = C_{nm}r_m(s,t) + S_{nm}i_m(s,t). \tag{46}
$$

The functions $r_m(s,t)$ and $i_m(s,t)$ are defined as

$$
\begin{aligned}
r_m(s,t) &= \mathrm{Re}(s+it)^m, \\
i_m(s,t) &= \mathrm{Im}(s+it)^m,
\end{aligned}
\tag{47}
$$

where

$$
\begin{aligned}
(s+it)^m &= (\cos\lambda\cos\varphi + \mathrm{i}\sin\lambda\cos\varphi)^m \\
&= e^{\mathrm{i}m\lambda}\cos^m\varphi.
\end{aligned}
\tag{48}
$$

r_m and i_m with $m = 0, 1, \ldots, N$ are determined recursively with

$$
\begin{aligned}
r_m &= sr_{m-1} - ti_{m-1}, \\
i_m &= si_{m-1} + tr_{m-1},
\end{aligned}
\tag{49}
$$

after inizialization with $r_0 = 1$, $i_0 = 0$. In this procedure, the $\cos^m\varphi$ factor, which is responsible for the singularities in the derivatives of the fnALFs at the geographic poles, is no longer bound to the SH function, but to r_m and i_m, which are never singular. This makes the gradients of V with respect to φ singularity-free.

In PN73 the sectorial Helmholtz polynomials are determined by means of an increasing degree-and-order recursion on the sectorial terms (i.e., $m = n$ with $n \geq 1$):

$$
H^n_n(u) = (2n-1)H^{n-1}_{n-1}(u), \tag{50}
$$

initialized with $H^0_0(u) = 1$ (which follows from $P_0 = 1$). The sub-diagonal elements (zonals and tesserals with $m = n-1$ and $n \geq 1$) are obtained through the recursion

$$
H^{n-1}_n(u) = uH^n_n(u). \tag{51}
$$

The remaining zonal and tesseral terms ($0 \leq m \leq n-2$) are computed through a mixed-strides recursion (MSR) formula (Fig. 3):

$$
H^m_n(u) = \left[uH^{m+1}_n(u) - H^{m+1}_{n-1}(u)\right] \Big/ (n-m), \tag{52}
$$

whereas, by definition,

$$
H^m_n(u) = 0, \quad m > n. \tag{53}
$$

In PN73 the first- and second-order derivatives of V with respect to x, y, z are obtained by application of the chain rule with respect to s, t, u, and r; then, appropriate mass coefficient functions for the several derivatives are introduced, and each gradient is the sum of a number of terms, each represented as a double summation, first over m and then over n, as is done in Eq. (44) for V itself. For the expressions of

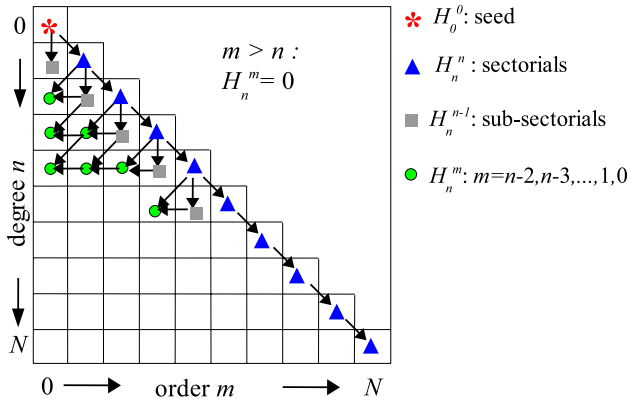

Fig. 3 Illustration of the mixed strides recursion algorithm proposed by PN73 for the evaluation of the HPs. In lower triangular part of the matrix, every square correspond specific combination of n and m. Away from the diagonal H_n^m is a linear combination of polynomials of different degree/order, therefore not on the same stride (*row/column*)

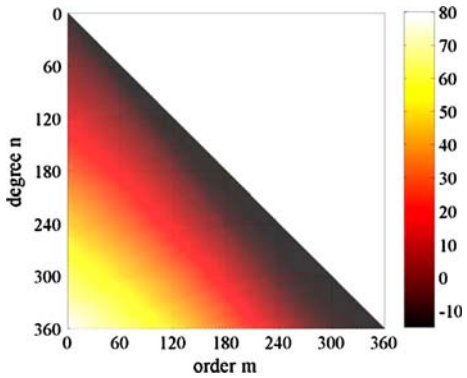

Fig. 4 Log_{10} of the difference between the fnHPs computed with the MSR algorithm and those resulting from adopti the IDR scheme: the difference grows with increasing degree (*downwards*) and decreasing order (*leftwards*), reaching values o order 80 at the zonals with highest degree. This shows that t MSR algorithm is highly unstable

such functions, the relations among them, and their role in the computation of the gravity gradients the reader is referred to PN73.

Follow-up work on PN73 is due to Spencer (1976) who made a complete revision, and Deprit (1979) who made a rearrangement of the PN73 algorithm on the basis of Horner's scheme. Then, the approach discussed by Balmino et al. (1990) is essentially equivalent to that of PN73, whereas Gottlieb (1993) developed a variant of PN73 based on Cartesian coordinates rather than direction cosines and geocentric distance of the field point. In the present contribution, the PN73 algorithm has been rewritten on the basis of the lumped coefficients approach with full normalization, and it has been extended to the third-order gradient.

The fully normalized Helmholtz polynomials (fnHPs) are defined as

$$\overline{H}_n^m(u) = \sqrt{(2-\delta_{o,m})(2n+1)\frac{(n-m)!}{(n+m)!}}H_n^m(u), \tag{54}$$

and the above recurrence relations [Eqs. (50), (51) and (52)] become

$$\begin{aligned}\overline{H}_n^n(u) &= \sqrt{\frac{(1+\delta_{1n})(2n+1)}{2n}}\overline{H}_{n-1}^{n-1}(u)\\ &\equiv f_n\overline{H}_{n-1}^{n-1}(u),\end{aligned} \tag{55}$$

$$\overline{H}_n^{n-1}(u) = u\sqrt{\frac{2n}{1+\delta_{1,n}}}\overline{H}_n^n(u), \tag{56}$$

and

$$\begin{aligned}\overline{H}_n^m(u) = &-\sqrt{\frac{(2n+1)(n-m-1)}{(1+\delta_{0,m})(2n-1)(n-m)}}\overline{H}_{n-1}^{m+1}(u)\\ &+u\sqrt{\frac{(n+m+1)}{(n-m)\left(1+\delta_{0,m}\right)}}\overline{H}_n^{m+1}(u),\end{aligned} \tag{57}$$

respectively. Experiments show that Eq. (57) is numerically unstable: Fig. 4 illustrates the fast increase with n of the difference between the fnHPs computed with the MSR algorithm and those obtained from the IDR scheme (cf. Sect. 3) (see also Lundberg and Schutz 1988):

$$\overline{H}_n^m(u) = ug_{nm}\overline{H}_{n-1}^m(u) - h_{nm}\overline{H}_{n-2}^m(u), \tag{58}$$

with g_{nm} and h_{nm} as in Eqs. (8) and (9), respectively.

The k^{th} derivative of the HP of degree n and order m is the HP of degree n and order $(m+k)$:

$$\frac{\mathrm{d}^k H_n^m(u)}{\mathrm{d}u^k} = H_n^{m+k}(u). \tag{59}$$

It can be shown by induction over the order of differentiation k, that its fully normalized form is

$$\frac{\mathrm{d}^k\overline{H}_n^m(u)}{\mathrm{d}u^k} = \left(k_{nm}k_{n,m+1},\ldots,k_{n,m+k-1}\right)\overline{H}_n^{m+k}(u), \tag{60}$$

with k_{nm} as in Eq. (11). In particular, the first derivative is

$$\frac{\mathrm{d}\overline{H}_n^m(u)}{\mathrm{d}u} = k_{nm}\overline{H}_n^{m+1}(u), \tag{61}$$

the second derivative is

$$\frac{\mathrm{d}^2\overline{H}_n^m(u)}{\mathrm{d}u^2} = k_{nm}k'_{n,m+1}\overline{H}_n^{m+2}(u), \tag{62}$$

and the third derivative is

$$\frac{\mathrm{d}^3\overline{H}_n^m(u)}{\mathrm{d}u^3} = k_{nm}k_{n,m+1}k_{n,m+2}\overline{H}_n^{m+3}(u). \tag{63}$$

Note that the recursions for the derivatives of the $\overline{H}_n^m$'s contain coefficients which do not depend on u, but only on n and m.

5.1 Lumped coefficients synthesis of the geopotential and its gradients

In this contribution, the *Pines* method has been rewritten in the lumped coefficients form. It can be easily shown that

$$V = \sum_{m=0}^{N} (A_m^{(1)} \cos m\lambda + B_m^{(1)} \sin m\lambda) \cos^m \varphi, \tag{64}$$

with $A_m^{(1)}$ and $B_m^{(1)}$ given by

$$A_m^{(1)} = \sum_{n=m}^{N} \rho_n \overline{C}_{nm} \overline{H}_n^m, \tag{65}$$

$$B_m^{(1)} = \sum_{n=m}^{N} \rho_n \overline{S}_{nm} \overline{H}_n^m. \tag{66}$$

As for the gradients, by application of the chain rule the differential operators of the gravitational potential V with respect to the global coordinates x, y, z of P can be written as a function of the differential operators with respect to r, s, t and u (see also PN73):

$$\begin{aligned}
\frac{\partial}{\partial x} &= \frac{1}{r}\frac{\partial}{\partial s} + s\left(\frac{\partial}{\partial r} - \frac{s}{r}\frac{\partial}{\partial s} - \frac{t}{r}\frac{\partial}{\partial t} - \frac{u}{r}\frac{\partial}{\partial u}\right),\\
\frac{\partial}{\partial y} &= \frac{1}{r}\frac{\partial}{\partial t} + t\left(\frac{\partial}{\partial r} - \frac{s}{r}\frac{\partial}{\partial s} - \frac{t}{r}\frac{\partial}{\partial t} - \frac{u}{r}\frac{\partial}{\partial u}\right),\\
\frac{\partial}{\partial z} &= \frac{1}{r}\frac{\partial}{\partial u} + u\left(\frac{\partial}{\partial r} - \frac{s}{r}\frac{\partial}{\partial s} - \frac{t}{r}\frac{\partial}{\partial t} - \frac{u}{r}\frac{\partial}{\partial u}\right).
\end{aligned} \tag{67}$$

By defining the operators

$$\begin{aligned}
L_1 &= \frac{1}{r}\frac{\partial}{\partial s},\\
L_2 &= \frac{1}{r}\frac{\partial}{\partial t},\\
L_3 &= \frac{1}{r}\frac{\partial}{\partial u},\\
L_4 &= \frac{\partial}{\partial r} - \frac{s}{r}\frac{\partial}{\partial s} - \frac{t}{r}\frac{\partial}{\partial t} - \frac{u}{r}\frac{\partial}{\partial u},
\end{aligned} \tag{68}$$

Eqs. (67) can be rewritten more concisely as

$$\begin{aligned}
\frac{\partial}{\partial x} &= L_1 + sL_4,\\
\frac{\partial}{\partial y} &= L_2 + tL_4,\\
\frac{\partial}{\partial z} &= L_3 + uL_4.
\end{aligned} \tag{69}$$

Hence, differentiating the geopotential V [Eq. (64)] with respect to global Cartesian coordinates yields the components of the first-order gradient (the notation of Casotto and Fantino (2008) has been used in representing the physical components of the gradients)

Table 10 The functions a_i $(i = 1, 2, 3, 4)$ in the *Pines* method. The quantities c_{m-j} and s_{m-j} with $j = 0, 1, 2, 3$ replace the expressions $\cos(m-j)\lambda$ and $\sin(m-j)\lambda$, respectively

$$\begin{aligned}
a_1 &= \sum_{m=1}^{N} m\left(A_m^{(1)} c_{m-1} + B_m^{(1)} s_{m-1}\right)\cos^{m-1}\varphi\\
a_2 &= \sum_{m=1}^{N} m\left(B_m^{(1)} c_{m-1} - A_m^{(1)} s_{m-1}\right)\cos^{m-1}\varphi\\
a_3 &= \sum_{m=0}^{N} \left(A_m^{(2)} c_m + B_m^{(2)} s_m\right)\cos^{m}\varphi\\
a_4 &= -\sum_{m=0}^{N} \left(A_m^{(3)} c_m + B_m^{(3)} s_m\right)\cos^{m}\varphi
\end{aligned}$$

$$\begin{aligned}
V_x &= a_1 + sa_4,\\
V_y &= a_2 + ta_4,\\
V_z &= a_3 + ua_4,
\end{aligned} \tag{70}$$

where the quantities a_j $(j = 1, 2, 3, 4)$ result from the application of the operators L_1, L_2, L_3 and L_4 to V, and their lumped coefficients expressions are given in Table 10. Note that in working out the espression of a_4, the following relation has been used:

$$\frac{\partial \rho_n}{\partial r} = -(n+1)\frac{\rho_{n+1}}{a} \equiv -(n+1)\frac{\rho_n}{r}. \tag{71}$$

Differentiation of Eq. (70) with respect to x, y and z provides the six physical components of the second-order gravity gradient $\nabla\nabla V$:

$$\begin{aligned}
V_{xx} &= a_{11} + 2sa_{14} + a_4/r + s^2 a_{44} - s^2 a_4/r,\\
V_{xy} &= a_{12} + sta_{44} + sa_{24} + ta_{14} - sta_4/r,\\
V_{yy} &= a_{22} + 2ta_{24} + a_4/r + t^2 a_{44} - t^2 a_4/r,\\
V_{xz} &= a_{13} + sua_{44} + sa_{34} + ua_{14} - sua_4/r,\\
V_{yz} &= a_{23} + tua_{44} + ta_{34} + ua_{24} - tua_4/r,\\
V_{zz} &= a_{33} + 2ua_{34} + a_4/r + u^2 a_{44} - u^2 a_4/r.
\end{aligned} \tag{72}$$

The a_{ij} $(i, j = 1, 2, 3, 4)$ functions are defined in Table 11.

Further differentiation provides the ten independent physical components of the third-order gravity gradient $\nabla\nabla\nabla V$:

$$\begin{aligned}
V_{xxx} &= a_{111} + 3sa_{114} + 3s^2 a_{441} + s^3 a_{444}\\
&\quad + (1-s^2)(a_{14}/r + sa_{44} - sa_4/r^2),\\
V_{xxy} &= a_{112} + 2sa_{124} + s^2 a_{442} + ta_{114} + 2tsa_{441}\\
&\quad + (1-s^2)a_{24}/r + t(1-3s^2)(a_{44} - a_4/r)/r\\
&\quad + ts^2 a_{444} - 2tsa_{14}/r,\\
V_{xxz} &= a_{113} + 2sa_{143} + s^2 a_{443} + ua_{114} + 2usa_{441}\\
&\quad + (1-s^2)a_{34}/r + u(1-3s^2)(a_{44} - a_4/r)/r\\
&\quad + us^2 a_{444} - 2usa_{14},
\end{aligned}$$

Table 11 The functions a_{ij} $(i, j = 1, 2, 3, 4)$ in the *Pines* method. The quantities c_{m-j} and s_{m-j} with $j = 0, 1, 2, 3$ replace the expressions $\cos(m-j)\lambda$ and $\sin(m-j)\lambda$, respectively

$$a_{11} = \sum_{m=1}^{N} m(m-1)\left(A_m^{(1)} c_{m-2} + B_m^{(1)} s_{m-2}\right)\cos^{m-2}\varphi \qquad a_{12} = \sum_{m=2}^{N} m(m-1)\left(B_m^{(1)} c_{m-2} - A_m^{(1)} s_{m-2}\right)\cos^{m-2}\varphi$$

$$a_{13} = \sum_{m=1}^{N} m\left(A_m^{(2)} c_{m-1} + B_m^{(2)} s_{m-1}\right)\cos^{m-1}\varphi \qquad a_{14} = -\sum_{m=1}^{N} m\left(A_m^{(3)} c_{m-1} + B_m^{(3)} s_{m-1}\right)\cos^{m-1}\varphi$$

$$a_{22} = -a_{11} \qquad a_{23} = \sum_{m=1}^{N} m\left(B_m^{(2)} c_{m-1} - A_m^{(2)} s_{m-1}\right)\cos^{m-1}\varphi$$

$$a_{24} = -\sum_{m=1}^{N} m\left(B_m^{(3)} c_{m-1} - A_m^{(3)} s_{m-1}\right)\cos^{m-1}\varphi \qquad a_{33} = \sum_{m=0}^{N}\left(A_m^{(4)} c_m + B_m^{(4)} s_m\right)\cos^{m}\varphi$$

$$a_{34} = -\sum_{m=0}^{N}\left(A_m^{(5)} c_m + B_m^{(5)} s_m\right)\cos^{m}\varphi \qquad a_{44} = \sum_{m=0}^{N}\left(A_m^{(6)} c_m + B_m^{(6)} s_m\right)\cos^{m}\varphi$$

$$\begin{aligned}
V_{yyx} &= a_{221} + 2ta_{124} + t^2 a_{441} + sa_{224} + 2tsa_{442} \\
&\quad + (1-t^2)a_{14}/r + s(1-3t^2)(a_{44} - a_4/r)/r \\
&\quad + t^2 sa_{444} - 2tsa_{24}/r, \\
V_{yyy} &= a_{222} + 3ta_{224} + 3t^2 a_{442} + t^3 a_{444} \\
&\quad + 3(1-t^2)(a_{24} + ta_{44} - ta_4/r)/r, \\
V_{yyz} &= a_{223} + 2ta_{243} + t^2 a_{443} + ua_{224} + 2tua_{442} \\
&\quad + (1-t^2)a_{34}/r + u(1-3t^2)(a_{44} - a_4/r)/r \\
&\quad + t^2 ua_{444} - 2tua_{24}/r, \\
V_{zzx} &= a_{331} + 2ua_{143} + u^2 a_{441} + sa_{334} + 2usa_{443} \\
&\quad + (1-u^2)a_{14}/r + s(1-3u^2)(a_{44} - a_4/r)/r \\
&\quad + u^2 sa_{444} - 2usa_{34}/r, \\
V_{zzy} &= a_{332} + 2ua_{243} + u^2 a_{442} + ta_{334} + 2uta_{443} \\
&\quad + (1-u^2)a_{24}/r + t(1-3u^2)(a_{44} - a_4/r)/r \\
&\quad + u^2 ta_{444} - 2uta_{34}/r, \\
V_{zzz} &= a_{333} + 3ua_{334} + 3u^2 a_{443} + u^3 a_{444} \\
&\quad + 3(1-u^2)(a_{34} + ua_{44} - ua_4/r)/r, \\
V_{xyz} &= a_{123} + ua_{124} + sa_{243} + usa_{442} + ta_{143} \\
&\quad + sta_{443} + usta_{444} - sta_{34} - usta_{44}/r \\
&\quad - usa_{24}/r - uta_{14}/r + 3usta_4/r^2 + uta_{441},
\end{aligned} \tag{73}$$

with a_{ijk} $(i, j, k = 1, 2, 3, 4)$ given in Table 12.

The expressions of the several lumped coefficients $A_m^{(i)}$, $B_m^{(i)}$ $(i = 1, 2, \ldots, 10)$ are given in Table 13, and the auxiliary functions $\overline{L}_n^m$, $\mathrm{d}\overline{L}_n^m$, $\mathrm{d}^2\overline{L}_n^m$, $\overline{O}_n^m$, $\overline{Q}_n^m$, and $\overline{W}_n^m$ that appear there, are defined in Table 14.

6 The method of Cunningham–Metris

By the name *Cunningham–Metris*, we denote a method for the computation of the derivatives of the geopotential in Cartesian coordinates within the global reference system which is originally due to CN70, and was later extended by MT99.

The algorithm developed by CN70 is based on the representation of the gravitational potential in solid spherical harmonics V_{nm}'s

$$V_{nm} \equiv \frac{\cos m\lambda + \mathrm{i}\sin m\lambda}{r^{n+1}} P_{nm}(\varphi), \tag{74}$$

through which the potential V takes the form

$$V = \mathrm{Re}\left[GM \sum_{n=0}^{N}\sum_{m=0}^{n} a^n (C_{nm} - \mathrm{i}S_{nm}) V_{nm}\right], \tag{75}$$

i being the imaginary unit.

The V_{nm}'s can be written as:

$$V_{nm} = \frac{(-1)^n}{(n-m)!}\left(\frac{\partial}{\partial x} + \mathrm{i}\frac{\partial}{\partial y}\right)^m \left(\frac{\partial}{\partial z}\right)^{n-m}\left(\frac{1}{l}\right) \tag{76}$$

for $n > m$, and

$$V_{nn} = (-1)^n \left(\frac{\partial}{\partial x} + \mathrm{i}\frac{\partial}{\partial y}\right)^n \left(\frac{1}{l}\right) \tag{77}$$

for $n = m$. They obey two IDR relations, one for sectorial harmonics,

$$V_{nn} = (2n-1)\left(\frac{x + \mathrm{i}y}{r^2}\right) V_{n-1,n-1}, \quad n \geq 1, \tag{78}$$

initialized with $V_{00} = 1/r$, one for the remaining terms

$$\begin{aligned}
(n-m)V_{nm} &= (2n-1)\left(\frac{z}{r^2}\right) V_{n-1,m} \\
&\quad - \left(\frac{n+m-1}{r^2}\right) V_{n-2,m}, \quad n \geq 1,
\end{aligned} \tag{79}$$

where $V_{n-2,m} \equiv 0$ for $n < 2$.

Successive application of the operators of differentiation $\partial/\partial z$ and $(\partial/\partial x + i\partial/\partial y)$ and further algebraic manipulations lead to the following expression for the derivatives of

Table 12 The functions a_{ijk} $(i, j, k = 1, 2, 3, 4)$ in the *Pines* method

$$a_{111} = \sum_{m=3}^{N} m(m-1)(m-2)\left(A_m^{(1)}c_{m-3} + B_m^{(1)}s_{m-3}\right)\cos^{m-2}\varphi$$

$$a_{112} = -a_{222}$$

$$a_{113} = \sum_{m=2}^{N} m(m-1)\left(A_m^{(2)}c_{m-2} + B_m^{(2)}s_{m-2}\right)\cos^{m-2}\varphi$$

$$a_{114} = -\sum_{m=2}^{N} m(m-1)\left(A_m^{(3)}c_{m-2} + B_m^{(3)}s_{m-2}\right)\cos^{m-2}\varphi$$

$$a_{123} = \sum_{m=2}^{N} m(m-1)\left(B_m^{(2)}c_{m-2} - A_m^{(2)}s_{m-2}\right)\cos^{m-2}\varphi$$

$$a_{124} = -\sum_{m=2}^{N} m(m-1)\left(B_m^{(3)}c_{m-2} - A_m^{(3)}s_{m-2}\right)\cos^{m-2}\varphi$$

$$a_{143} = -\sum_{m=2}^{N} m\left(A_m^{(5)}c_{m-1} + B_m^{(5)}s_{m-1}\right)\cos^{m-1}\varphi$$

$$a_{221} = -a_{111}$$

$$a_{222} = -\sum_{m=3}^{N} m(m-1)(m-2)\left(B_m^{(1)}c_{m-3} - A_m^{(1)}s_{m-3}\right)\cos^{m-2}\varphi$$

$$a_{223} = -a_{113}$$

$$a_{224} = -a_{114}$$

$$a_{243} = -\sum_{m=1}^{N} m\left(B_m^{(5)}c_{m-1} - A_m^{(5)}s_{m-1}\right)\cos^{m-1}\varphi$$

$$a_{331} = \sum_{m=1}^{N} m\left(A_m^{(4)}c_{m-1} + B_m^{(4)}s_{m-1}\right)\cos^{m-1}\varphi$$

$$a_{332} = \sum_{m=1}^{N} m\left(B_m^{(4)}c_{m-1} - A_m^{(4)}s_{m-1}\right)\cos^{m-1}\varphi$$

$$a_{333} = \sum_{m=0}^{N}\left(A_m^{(7)}c_m + B_m^{(7)}s_m\right)\cos^{m}\varphi$$

$$a_{334} = -\sum_{m=0}^{N}\left(A_m^{(8)}c_m + B_m^{(8)}s_m\right)\cos^{m}\varphi$$

$$a_{441} = \sum_{m=1}^{N} m\left(A_m^{(6)}c_{m-1} + B_m^{(6)}s_{m-1}\right)\cos^{m-1}\varphi$$

$$a_{442} = \sum_{m=1}^{N} m\left(B_m^{(6)}c_{m-1} - A_m^{(6)}s_{m-1}\right)\cos^{m-1}\varphi$$

$$a_{443} = \sum_{m=0}^{N}\left(A_m^{(9)}c_m + B_m^{(9)}s_m\right)\cos^{m}\varphi$$

$$a_{444} = -\sum_{m=1}^{N} m\left(A_m^{(10)}c_{m-1} + B_m^{(10)}s_{m-1}\right)\cos^{m-1}\varphi$$

The quantities c_{m-j} and s_{m-j} with $j = 0, 1, 2, 3$ replace the expressions $\cos(m-j)\lambda$ and $\sin(m-j)\lambda$, respectively

arbitrary order α, β and γ in x, y, and z respectively (global Cartesian coordinates):

$$\frac{\partial^{\eta} V_{nm}}{\partial x^{\alpha}\partial y^{\beta}\partial z^{\gamma}} = \mathrm{i}^{\beta}\sum_{j=0}^{\alpha+\beta}\frac{(-1)^{\alpha+\gamma-j}}{2^{\alpha+\beta}}\frac{(n-m+\gamma+2j)!}{(n-m)!} \times C_{\alpha\beta j}\, V_{n+\eta,m+\alpha+\beta-2j}, \tag{80}$$

in which $\eta = \alpha + \beta + \gamma$,

$$C_{\alpha\beta j} = \sum_{k}(-1)^{k}\binom{\alpha}{j-k}\binom{\beta}{k} \tag{81}$$

and

$$\max(0, j-\alpha) \le k \le \min(\beta, j). \tag{82}$$

Eq. (80) shows that the derivatives of any V_{nm} are simply linear combinations of other V_{nm}'s. Therefore, by application of the IDR scheme represented by Eqs. (78) and (79), all the V_{nm}'s up to degree $N + \eta$ and order $N + \alpha + \beta$ are computed, stored and then employed in the determination of the derivatives $\partial^{\eta} V_{nm}/\partial x^{\alpha}\partial y^{\beta}\partial z^{\gamma}$.

In Montenbruck and Gill (2000), the CN70 algorithm is employed in the computation of the components of the partial derivatives of the Earth's attraction with respect to position, in a discussion on the variational equations of the state transition matrix within a statistical orbit determination. Gill et al. (2000) achieved an efficient computation of spacecraft acceleration using the CN70 algorithm in the context of a navigation system study. Arsov and Pail (2003) applied the relations proposed in CN70 to the numerical integration of the orbit and variational equations in the evaluation of satellite-to-satellite tracking observations for gravity field determination from GOCE.

The algorithm presented in MT99 is effectively the completion of CN70, as it provides the gravity gradient of order α, β and γ in x, y and z respectively, through the harmonic synthesis

$$\frac{\partial^{\eta} V}{\partial x^{\alpha}\partial y^{\beta}\partial z^{\gamma}} = \frac{GM}{a^{1+\eta}}\sum_{n=\eta}^{N+\eta}\sum_{m=0}^{n-\gamma}\left[\overline{C}_{nm}^{(\alpha\beta\gamma)}\overline{H}_{nm}^{R} + \overline{S}_{nm}^{(\alpha\beta\gamma)}\overline{H}_{nm}^{I}\right], \tag{83}$$

where $\overline{H}_{nm}^{R}$ and $\overline{H}_{nm}^{I}$ are the real and imaginary parts of the function $\overline{H}_{nm}(X, Y, Z)$, obtained by applying a complex differential operator to $1/R$, the ratio $R = r/a$ of the geocentric distance to the observation point and the mean Earth's radius (or any scaling distance pertaining to the set of geopotential coefficients):

$$\overline{H}_{nm} = \alpha_{nm}\left(\frac{\partial}{\partial X} + \mathrm{i}\frac{\partial}{\partial Y}\right)^{m}\left(\frac{\partial}{\partial Z}\right)^{n-m}\left(\frac{1}{R}\right). \tag{84}$$

Table 13 Definition of the lumped coefficients in the *Pines* method

$$A_m^{(1)} = \sum_{\substack{n=m\\N}}^{N} \rho_n \overline{C}_{nm} \overline{H}_n^m \qquad B_m^{(1)} = \sum_{\substack{n=m\\N}}^{N} \rho_n \overline{S}_{nm} \overline{H}_n^m$$
$$A_m^{(2)} = \sum_{\substack{n=m\\N}}^{N} \rho_n \overline{C}_{nm} \overline{H}_n^m / \mathrm{d}u \qquad B_m^{(2)} = \sum_{\substack{n=m\\N}}^{N} \rho_n \overline{S}_{nm} \mathrm{d}\overline{H}_n^m / \mathrm{d}u$$
$$A_m^{(3)} = \sum_{\substack{n=m\\N}}^{N} \rho_n \overline{C}_{nm} \overline{L}_n^m \qquad B_m^{(3)} = \sum_{\substack{n=m\\N}}^{N} \rho_n \overline{S}_{nm} \overline{L}_n^m$$
$$A_m^{(4)} = \sum_{\substack{n=m\\N}}^{N} \rho_n \overline{C}_{nm} \mathrm{d}^2\overline{H}_n^m / \mathrm{d}u^2 \qquad B_m^{(4)} = \sum_{\substack{n=m\\N}}^{N} \rho_n \overline{S}_{nm} \mathrm{d}^2\overline{H}_n^m / \mathrm{d}u^2$$
$$A_m^{(5)} = \sum_{\substack{n=m\\N}}^{N} \rho_n \overline{C}_{nm} \mathrm{d}\overline{L}_n^m \qquad B_m^{(5)} = \sum_{\substack{n=m\\N}}^{N} \rho_n \overline{S}_{nm} \mathrm{d}\overline{L}_n^m$$
$$A_m^{(6)} = \sum_{\substack{n=m\\N}}^{N} \rho_n \overline{C}_{nm} \overline{O}_n^m \qquad B_m^{(6)} = \sum_{\substack{n=m\\N}}^{N} \rho_n \overline{S}_{nm} \overline{O}_n^m$$
$$A_m^{(7)} = \sum_{\substack{n=m\\N}}^{N} \rho_n \overline{C}_{nm} \mathrm{d}^3\overline{H}_n^m / \mathrm{d}u^3 \qquad B_m^{(7)} = \sum_{\substack{n=m\\N}}^{N} \rho_n \overline{S}_{nm} \mathrm{d}^3\overline{H}_n^m / \mathrm{d}u^3$$
$$A_m^{(8)} = \sum_{\substack{n=m\\N}}^{N} \rho_n \overline{C}_{nm} \mathrm{d}^2\overline{L}_n^m \qquad B_m^{(8)} = \sum_{\substack{n=m\\N}}^{N} \rho_n \overline{S}_{nm} \mathrm{d}^2\overline{L}_n^m$$
$$A_m^{(9)} = \sum_{\substack{n=m\\N}}^{N} \rho_n \overline{C}_{nm} \overline{Q}_n^m \qquad B_m^{(9)} = \sum_{\substack{n=m\\N}}^{N} \rho_n \overline{S}_{nm} \overline{Q}_n^m$$
$$A_m^{(10)} = \sum_{\substack{n=m\\N}}^{N} \rho_n \overline{C}_{nm} \overline{W}_n^m \qquad B_m^{(10)} = \sum_{\substack{n=m\\N}}^{N} \rho_n \overline{S}_{nm} \overline{W}_n^m$$

X, Y, Z are the dimensionless coordinates of the field point:

$$\begin{aligned} X &= x/a, \\ Y &= y/a, \\ Z &= z/a, \end{aligned} \tag{85}$$

and α_{nm} is the full normalization factor:

$$\alpha_{nm} = (-1)^n \sqrt{\frac{(2n+1)(2-\delta_{0m})}{(n+m)!(n-m)!}}. \tag{86}$$

The functions $\overline{H}_{nm}^R$ and $\overline{H}_{nm}^I$ are computed by IDR on the amplitude $\overline{E}_{nm}$ defined through

$$\overline{H}_{nm}^R + \mathrm{i}\overline{H}_{nm}^I = \overline{E}_{nm} \exp(\mathrm{i}m\lambda) \tag{87}$$

via the sequence

$$\overline{E}_{00} = \frac{1}{R}, \tag{88}$$

$$\overline{E}_{11} = \sqrt{3}\frac{\rho}{R^2}\overline{E}_{00}, \tag{89}$$

$$\overline{E}_{mm} = \sqrt{\frac{2m+1}{2m}}\frac{\rho}{R^2}\overline{E}_{m-1,m-1}, \tag{90}$$

$$\overline{E}_{m+1,m} = \sqrt{2m+3}\frac{Z}{R^2}\overline{E}_{mm}, \tag{91}$$

$$\overline{E}_{nm} = g_{nm}\left[\frac{Z}{R^2}\overline{E}_{n-1,m} - \frac{1}{g_{n-1,m}R^2}\overline{E}_{n-2,m}\right], \tag{92}$$

with $\rho = \sqrt{X^2+Y^2}$ and g_{nm} as in Eq. (8).

The functions $\overline{C}_{nm}^{(\alpha\beta\gamma)}$ and $\overline{S}_{nm}^{(\alpha\beta\gamma)}$ in Eq. (83) are appropriate combinations of the Stokes coefficients of the gravity field:

$$\begin{aligned} \overline{C}_{nm}^{(\alpha\beta\gamma)} = \frac{(-1)^{\beta/2}}{(-2)^{\alpha+\beta}} \sum_{p=0}^{\alpha}\sum_{q=0}^{\beta} \big[&\varepsilon^+ A^+ \overline{C}_{n-\eta,m+\sigma} \\ &+ (1-\delta_{0m})\varepsilon^- A^- \overline{C}_{n-\eta,-m+\sigma}\big], \end{aligned} \tag{93}$$

$$\begin{aligned} \overline{S}_{nm}^{(\alpha\beta\gamma)} = \frac{(-1)^{\beta/2}}{(-2)^{\alpha+\beta}} \sum_{p=0}^{\alpha}\sum_{q=0}^{\beta} \big[&\varepsilon^+ A^+ \overline{S}_{n-\eta,m+\sigma} \\ &+ (1-\delta_{0m})\varepsilon^- A^- \overline{S}_{n-\eta,-m+\sigma}\big], \end{aligned} \tag{94}$$

for j even, and

$$\begin{aligned} \overline{C}_{nm}^{(\alpha\beta\gamma)} = \frac{(-1)^{(\beta-1)/2}}{(-2)^{\alpha+\beta}} \sum_{p=0}^{\alpha}\sum_{q=0}^{\beta} \big[&\varepsilon^+ A^+ \overline{S}_{n-\eta,m+\sigma} \\ &+ (1-\delta_{0m})\varepsilon^- A^- \overline{S}_{n-\eta,-m+\sigma}\big], \end{aligned} \tag{95}$$

$$\begin{aligned} \overline{S}_{nm}^{(\alpha\beta\gamma)} = \frac{(-1)^{(\beta-1)/2}}{(-2)^{\alpha+\beta}} \sum_{p=0}^{\alpha}\sum_{q=0}^{\beta} \big[&-\varepsilon^+ A^+ \overline{C}_{n-\eta,m+\sigma} \\ &+ (1-\delta_{0m})\varepsilon^- A^- \overline{C}_{n-\eta,-m+\sigma}\big], \end{aligned} \tag{96}$$

for j odd. σ replaces the expression $\alpha+\beta-2p-2q$, whereas

Table 14 *Pines* method: definition of the auxiliary functions that appear in the expressions of the lumped coefficients

$$\overline{L}_n^m = (n+m+1)\overline{H}_n^m + u d\overline{H}_n^m/\mathrm{d}u$$
$$\mathrm{d}\overline{L}_n^m = (n+m+2)d\overline{H}_n^m/\mathrm{d}u + u\mathrm{d}^2\overline{H}_n^m/\mathrm{d}u^2$$
$$\mathrm{d}^2\overline{L}_n^m = (n+m+3)\mathrm{d}^2\overline{H}_n^m/\mathrm{d}u^2 + u\mathrm{d}^3\overline{H}_n^m/\mathrm{d}u^3$$
$$\overline{O}_n^m = (n+m+1)(n+m+2)\overline{H}_n^m + 2u(n+m+2)d\overline{H}_n^m/\mathrm{d}u + u^2\mathrm{d}^2\overline{H}_n^m/\mathrm{d}u^2$$
$$\overline{Q}_n^m = (n+m+2)(n+m+3)d\overline{H}_n^m/\mathrm{d}u + 2u(n+m+3)\mathrm{d}^2\overline{H}_n^m/\mathrm{d}u^2 + u^2\mathrm{d}^3\overline{H}_n^m/\mathrm{d}u^3$$
$$\overline{W}_n^m = (n+m+1)(n+m+2)(n+m+3)\overline{H}_n^m + 3u(n+m+2)(n+m+3)d\overline{H}_n^m/\mathrm{d}u$$

$$A^{+} = (-1)^{p} \binom{\alpha}{p} \binom{\beta}{q} \frac{\alpha_{n-\eta,m+\sigma}}{\alpha_{nm}}, \tag{97}$$

$$A^{-} = (-1)^{m+p} \binom{\alpha}{p} \binom{\beta}{q} \frac{\alpha_{n-\eta,m-\sigma}}{\alpha_{nm}}, \tag{98}$$

$$\varepsilon^{+} = \begin{cases} 1 & \text{if } \begin{cases} 2p+2q \geq -n+m+2\alpha+2\beta+\gamma \\ 2p+2q \leq m+\alpha+\beta \end{cases} \\ 0 & \text{otherwise,} \end{cases} \tag{99}$$

$$\varepsilon^{-} = \begin{cases} 1 & \text{if } \begin{cases} 2p+2q \geq -n-m+2\alpha+2\beta+\gamma \\ 2p+2q \leq -m+\alpha+\beta \end{cases} \\ 0 & \text{otherwise.} \end{cases} \tag{100}$$

Like *Pines*, *Cunningham–Metris* offers a singularity-free representation of the gravity gradients. However, its major value is the generality of the formulation, which is the same for the derivative of any order.

6.1 Lumped coefficients synthesis of the geopotential and its gradients

In this contribution, the MT99 formulation of the geopotential and its gradients [Eq. 83] has been rewritten in the lumped coefficients form:

$$\frac{\partial^{\eta} V}{\partial x^{\alpha} \partial y^{\beta} \partial z^{\gamma}} = \frac{GM}{a^{1+\eta}} \sum_{m=0}^{N+3\eta} \left(A_m^{(\alpha\beta\gamma)} \cos m\lambda + B_m^{(\alpha\beta\gamma)} \sin m\lambda \right), \tag{101}$$

where the gravity gradient of order α, β, and γ in x, y, and z respectively, requires a specific set of lumped coefficients, $A_m^{(\alpha\beta\gamma)}$ and $B_m^{(\alpha\beta\gamma)}$ (with $m = 0,1,2,\ldots,N+3\eta$):

$$A_m^{(\alpha\beta\gamma)} = \sum_{n=m}^{N+3\eta} \overline{C}_{nm}^{(\alpha\beta\gamma)} \overline{E}_{nm}, \tag{102}$$

$$B_m^{(\alpha\beta\gamma)} = \sum_{n=m}^{N+3\eta} \overline{S}_{nm}^{(\alpha\beta\gamma)} \overline{E}_{nm}. \tag{103}$$

The $\overline{E}_{nm}$'s [Eqs. (88)–(92)] depend on geocentric distance (R) and geographic latitude (φ) only. Therefore, when the observation points are located at the nodes of a regular, spherical grid, each $\overline{E}_{nm}$ needs to be computed only once per parallel, thus offering improved performances over the original version [Eq. 83].

7 Numerical tests

Four software codes, named *LEGENDRE*, *CLENSHAW*, *PINES*, and *METRIS*, have been developed in Fortran95 to perform the computations prescribed by the corresponding four methods:

1. *LEGENDRE* executes IDR on fnALFs [Eqs. 5 and 7], computes their derivatives [Eqs. 10, 12 and 13], and applies the lumped coefficients approach to the synthesis of the geopotential and its gradients in the local reference system (Sect. 3.1).
2. *CLENSHAW* implements the Clenshaw summation on the fnALFs with the lumped coefficients approach and the IDR recursion on the fnALFs and their derivatives (Sect. 4) to finally yield the geopotential and its gradients in the local reference system.
3. *PINES* performs IDR on fnHPs [Eqs. 55 and 58], computes their derivatives [Eqs. 61, 62 and 63], and applies the lumped coefficients approach to the synthesis of the geopotential and its gradients in the global reference system (Sect. 5.1).
4. *METRIS* executes the *Cunningham–Metris* algorithm (Sect. 6). Its implementation is based on the Fortran 77 code made public by MT99 at http://wwwrc.obs-azur.fr/cerga/mecanique/potential/ as far as the core computations are concerned, i.e., the IDR recursions [Eqs. (88)–(92)] for the $\overline{E}_{nm}$ functions, and the computation of the Stokes coefficients and related quantities for the gradients [Eqs. (93)–(100)]. The code language, its architecture and the arrangement of the computations have been entirely changed and the lumped coefficients approach [Eqs. (101)–(103)] for geopotential and gravity gradients synthesis has been adopted. The results are expressed in the global reference system.

From the implementation point of view, the four codes are based on the same architecture and employ similar, if not identical, data structures (except for *METRIS*, which still implements some of the original multi-dimensional arrays for storing, e.g., the $C_{nm}^{(\alpha\beta\gamma)}$'s and $S_{nm}^{(\alpha\beta\gamma)}$'s). Dynamic memory is used for large vectors and arrays, and the precision assigned to the floating point variables is either IEEE (Institute of Electrical and Electronic Engineers) double or quadruple (set through a compilation parameter). The logical flow is common to the four codes: the input provided is essentially the gravitational field model (a set of fully normalized Stokes coefficients $\overline{C}_{nm}$, $\overline{S}_{nm}$ $(n, m = 0, 1, \ldots, N)$, the gravitational parameter GM and the associated scale length a) and the coordinates (x_i, y_i, z_i) or $(\lambda_i, \varphi_i, r_i)$ of N_{obs} observation points P_i, $i = 1, 2, \ldots, N_{\text{obs}}$. The normalization coefficients and all the coordinate-independent functions are computed first; then, two nested loops arrange the algorithm-specific computations according to latitude (outer loop) and longitude (inner loop) respectively, thus offering higher efficiency when the distribution of the field points form an equiangular grid.

The relative merits of the four algorithms have been assessed by testing the efficiency, precision and accuracy of the

corresponding codes. The efficiency tests compare the execution (CPU) times of the algorithms. The tests of numerical precision verify the numerical agreement among corresponding values of the gravitational potential V, the three components of ∇V, six components of $\nabla\nabla V$ and ten components of $\nabla\nabla\nabla V$ as computed by the four codes with the above mentioned machine precision levels, i.e., double and quadruple floating point precision; following the notation of the standard Fortran language (e.g., Ellis et al. 1994), these are referred to as REAL*8 and REAL*16, respectively. Finally, the tests of accuracy employ exact analytic identities to validate each algorithm both independently and relative to the others.

For all four codes, an interface enables the user to select the simulation parameters: the intervals $(0, N)$ and $(0, M)$ of spherical harmonic degrees and orders to be considered, the gravitational field model, and the spacial configuration of the observation points, which can be:

- GRID: (portion of) spherical grid at height h over the Earth's surface, extending over the longitude and latitude intervals (λ_s, λ_f) and (φ_s, φ_f) with cell size $\Delta\lambda$ and $\Delta\varphi$ in longitude and latitude respectively;
- ORBIT: three-dimensional positions on a satellite orbit.

These two options allow to explore the capabilities of the algorithms under different operating conditions: the GRID mode allows to exploit the latitude dependence of some of the functions present in the algorithms (which are therefore computed once per parallel of latitude), whereas simulations of type ORBIT require that all computations are repeated at every new field point.

Both types of input configuration find frequent application in the algorithms for gradiometric data inversion: some of the so-called *space-wise* methods (Rummel and Colombo 1985; Albertella et al. 2000; Migliaccio et al. 2004, 2006) are based on the averaging of the gradiometric observations inside blocks of an equiangular global grid, whereas *time-wise* methods (Koop 1993; Koop et al. 2000; Sneeuw 2000; Pail et al. 2005, 2006) exploit the properties of the time distribution of the measurements along the orbit.

Several simulation configurations based on either of the above two types were devised and named GRID1, GRID2, GRID3, ORBIT1 and ORBIT2 (see Table 15). Each configuration is tailored to the characteristics of the specific numerical test in which it is employed. The gravity model used in all configurations is EGM96 (Lemoine et al. 1998).

ORBIT1 and ORBIT2 (the orbital parameters of which are similar to those of the gradiometric mission GOCE: inclination $i = 96.5°$, eccentricity $e = 0.002$, height $h = 250\,\text{km}$) are uniformly sampled at time intervals equal to T_{res}, over a total mission duration ΔT (Fig. 5). They differ by the sampling interval, of 32 s and 1 s, respectively, the latter matching the resolution of the GOCE gradiometric measurements. The total number of observation points is 64 440 and $\approx 2 \times 10^6$, respectively.

Table 15 Five simulation configurations for the execution of the numerical tests on the four algorithms (see text)

	GRID1	GRID2	GRID3	ORBIT1	ORBIT2
h (km)	250.0	250.0	250.0	250.0	250.0
λ_s (°)	−179.0	−179.0	−107.0	–	–
λ_f (°)	180.0	145.0	−107.0	–	–
$\Delta\lambda$ (°)	1.0	36.0	0.0	–	–
ϕ_s (°)	−89.0	−89.0	86.00	–	–
ϕ_f (°)	89.0	89.0	89.95	–	–
$\Delta\phi$ (°)	1.0	1.0	0.05	–	–
N_{obs}	64 440	1 790	20	64 440	$\approx 2 \times 10^6$
gr. model	EGM96	EGM96	EGM96	EGM96	EGM96
N_1	0	0	0	0	0
N_2	360	360	360	360	360
M_1	0	0	0	0	0
M_2	360	360	360	360	360
e	–	–	–	0.002	0.002
i (°)	–	–	–	96.5	96.5
T_{res} (s)	–	–	–	31.0	1.0

Height h is above the EGM96 reference radius $a_e = 6378136.3$ m

The numerical tests have been run on a 2 GHz, 64-bit, single-processor, AMD Opteron platform with 2 GByte of RAM, and the compiler used is Intel f90 (version 10.0.023) under Linux Gentoo.

7.1 Efficiency

The numerical efficiency tests compare the execution (CPU) times of the four codes over GRID1 and ORBIT1 (Table 16; Figs. 6, 7). Multiplication of the CPU times of ORBIT1 by the factor 31 provides an extrapolated estimate of the performance of ORBIT2, since the orbit type is essentially a single-point simulation. GRID1 and ORBIT1 are made up of equal numbers of data points, and are therefore well-suited for investigating the effects of different input arrangements on the performance of the four codes. The execution times presented here do not include input/output (I/O) operations. The machine floating-point precision adopted for the numerical efficiency tests is REAL*8.

The efficiency tests have been executed four times on each code, i.e., for computing the geopotential only (V), then for the geopotential and its first-order gradient (i.e., V and ∇V), then up to the second-order gradient (i.e., V, ∇V and $\nabla\nabla V$) and finally for the geopotential and all the gradients of order one to three (i.e., V, ∇V, $\nabla\nabla V$ and $\nabla\nabla\nabla V$). The four tests have been carried out on each simulation type (i.e., GRID1 and ORBIT1).

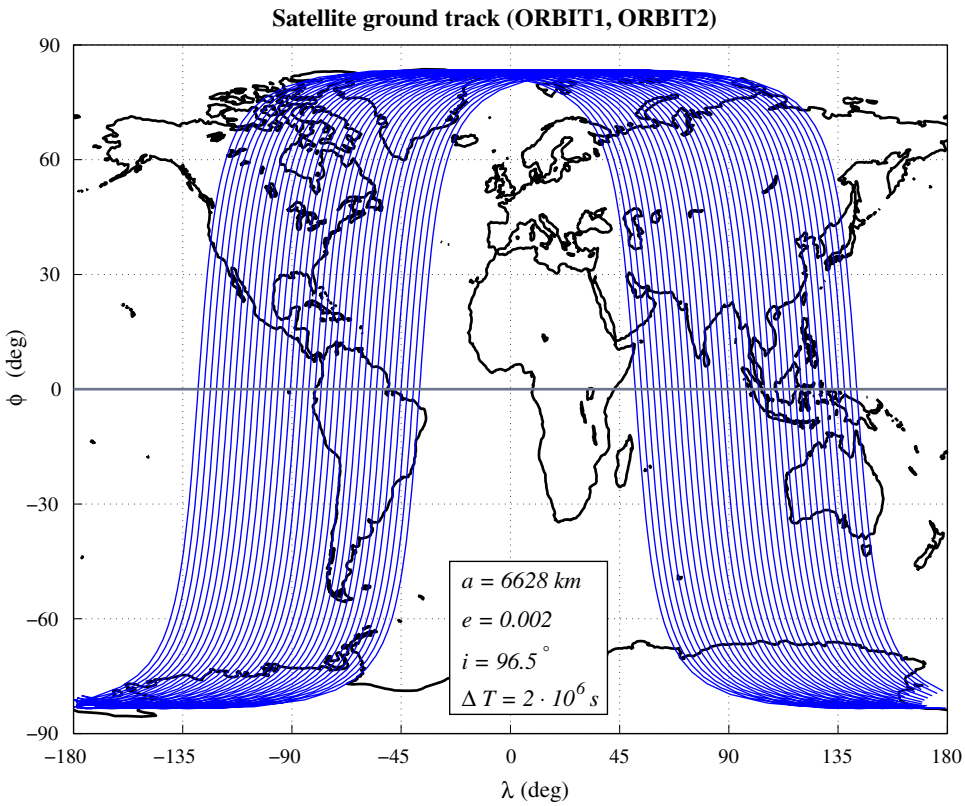

Fig. 5 Ground track of a simulated satellite orbit over the surface of the Earth. The orbital parameters (semi-major axis a, eccentricity e, inclination i) are those of the gradiometric satellite GOCE. $\Delta T \approx 2 \times 10^6$ s is the total mission duration of both ORBIT1 and ORBIT2, the difference being the sampling interval of 32 and 1 s, respectively

Table 16 Execution (CPU) times in seconds over GRID1 and ORBIT1 (see text)

Input	GRID1				ORBIT1			
Output	V	V ∇V	V ∇V $\nabla\nabla V$	V ∇V $\nabla\nabla V$ $\nabla\nabla\nabla V$	V	V ∇V	V ∇V $\nabla\nabla V$	V ∇V $\nabla\nabla V$ $\nabla\nabla\nabla V$
LEGENDRE	0.85	1.70	2.59	3.90	172.27	390.16	603.30	854.53
CLENSHAW	0.77	1.37	2.87	5.79	160.76	271.29	492.49	765.32
PINES	0.85	1.97	3.51	5.67	192.85	423.21	681.98	919.54
METRIS	0.92	2.41	5.17	9.75	220.59	540.16	1242.73	2329.13

The computation of the gradient of a given order is preceded by the synthesis of all the gradients of lower order, as suggested by the structure of the four algorithms and their implementation: the computation of quantities that are common among gradients of different order are computed only once. Finally, owing to the symmetry properties of the second- and third-order gravity gradients, $\nabla\nabla V$ is completely defined by six components, i.e., the three diagonal and three off-diagonal elements, and $\nabla\nabla\nabla V$ by ten. In the case of the second-order gravity gradient, though, additional time savings can be obtained by further restricting the computations to the non-redundant components, i.e., the three off-diagonal elements and any two of the diagonal elements, and then exploiting the null property of the Laplacian to compute the remaining diagonal element: more specifically, in the case of *LEGENDRE* avoiding the second differentiation with respect to φ ($V^*_{\varphi\varphi}$) should be the most favourable choice in terms of performance because it avoids the computation of the second-order derivatives of the ALFs.

The adopted compiler optimization option for the efficiency tests is -O2: it enables optimizations for speed, including global code scheduling, software pipelining, predication, and speculation. This is the generally recommended optimization level. In this respect, a major remark should be made before presenting and commenting any result: experiments made with the four codes show that disabling the compiler optimization flag may even increase the execution speed. Because of this, and since this contribution is

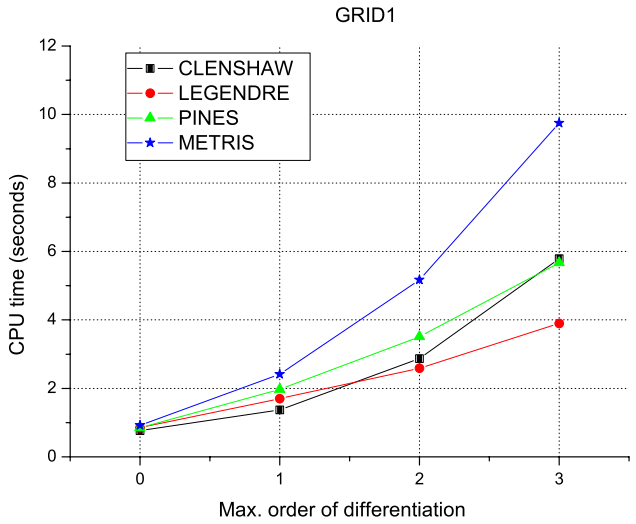

Fig. 6 CPU times (in seconds) required by the four codes for the computation of the geopotential and various combinations of its gradients of order one to three over GRID1. This plot is based on the data of Table 16

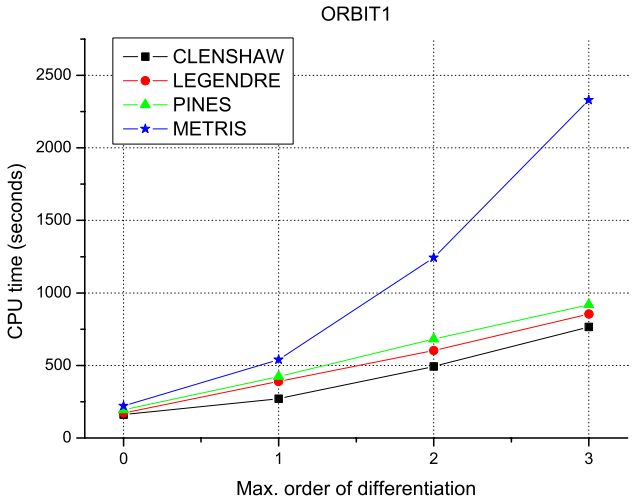

Fig. 7 CPU times (in seconds) required by the four codes for the computation of the geopotential and various combinations of its gradients of order one to three over ORBIT1. This plot is base on the data of Table 16

not meant as a study on compilers and code optimization, the -O2 flag has been left enabled throughout the efficiency tests, with the warning that the resulting CPU times and the consequent assessment of the relative merits of the four codes may change under different compilation options. The CPU times that are presented here should therefore be considered as indications of the order of magnitude of the time required by the several codes to perform the gravity gradient synthesis over the selected simulation configurations.

Table 16, Figs. 6 and 7 illustrate the performance levels of the four codes over GRID1 and ORBIT1. An overall agreement appears over GRID1, whereas ORBIT1 highlights a certain spread between the triple *CLENSHAW–LEGENDRE–PINES* and *METRIS*, which grows with increasing order of differentiation. The observed differences in CPU time do not necessarily reflect in the number of operations executed: Table 17 shows, e.g., that on ORBIT1 *CLENSHAW* and *METRIS* compute similar amounts of operations in all cases, but the latter performs three times worse than the former when the third-order derivatives are reached. In *METRIS*, a larger amount of memory is allocated with respect to the other codes, and this is eventually a consequence of the generality of the algorithm. Then, the use of multi-dimensional arrays rather than vectors, results in a slower and less efficient access to the memory. These two aspects may reasonably be the cause of the deterioration of its performance by a factor of three with respect to the fastest codes.

7.2 Relative precision

In principle, the correct and appropriate way to determine the precision of a computer code would be to compare its results with the *true* values of the computed quantities. In the case at hand, no truth values are available as a reference, and only an assessment of the "relative" numerical precision of the four codes can be made. In fact, the only really significant comparison is an "internal comparison", i.e., one which considers the results obtained by running each code on a given set of observation points in two different machine precision modes: comparisons have been made between the double (REAL*8) and the quadruple (REAL*16) floating

Table 17 Number of operations in units of 10^9 performed by the four codes over GRID1 and ORBIT1 (see text)

Input	GRID1				ORBIT1			
Output	V	V ∇V	V ∇V $\nabla\nabla V$	V ∇V $\nabla\nabla V$ $\nabla\nabla\nabla V$	V	V ∇V	V ∇V $\nabla\nabla V$	V ∇V $\nabla\nabla V$ $\nabla\nabla\nabla V$
LEGENDRE	0.129	0.409	0.992	1.987	29.545	71.744	147.768	270.297
CLENSHAW	0.141	0.618	1.725	3.789	25.358	88.540	194.132	334.202
PINES	0.153	0.607	1.608	3.428	29.569	76.141	177.753	380.817
METRIS	0.141	0.451	1.093	2.223	33.685	85.641	191.555	371.758

point precision versions of each code with the aim of assessing the numerical precision of the double relative to the quadruple precision mode.

The measure of relative precision of two numbers s_1 and s_2 has been taken as the number of significant figures they have in common. If we suggestively designate this measure as CD (common digits), then

$$\mathrm{CD} = \log_{10} \left| \frac{s_2}{s_1 - s_2} \right| . \tag{104}$$

Apart from the sign, this is also the approach adopted by Holmes and Featherstone (2002a,b). The non-integer nature of CD is symptomatic of the fact that the difference between two numbers is not in general a power of 10. If one insists on providing an integer number of common significant digits, then the most accurate statement would have to refer to the binary representation of the numbers, since that is the "longest" representation possible.

The adopted simulation configuration for the relative numerical precision tests is GRID2, a $36° \times 1°$ cell spherical grid (see Table 15): Figs. 1, 2, 3, and 4 of the ESM give the number of common significant digits between two given sets of results for every gravity gradient component as a function of latitude (each point in the plot is effectively an average over the number of points in which every parallel is divided), supplemented by an estimate of the average agreement over the entire grid.

The average numerical precision of *CLENSHAW**8 relative to *CLENSHAW**16 is approximately located between 13 and 16 digits. A very similar behaviour characterizes the numerical agreement between *LEGENDRE**8 and its quadruple precision counterpart. *PINES**8 shows average values always above 14, but some plots exhibit deep local minima, as low as nine digits, around latitude 0°. Such feature was already noted by Bettadpur et al. (1992). This behaviour is not intrinsic to the specific algorithms, but is a direct consequence of the reference system adopted; it affects only the components involving derivatives with respect to z because such quantities are characterized by a decrease of their absolute value at the equator, due to the vanishing of the monopolar term contribution. The global averages of the numerical precision of *METRIS* are all located around 14 digits, with local minima down to nine digits around latitude 0° as in the case of *PINES*.

Several components of the first-, second- and third-order gradients are singular at the geographic poles when computed with *CLENSHAW* and *LEGENDRE*. This is partly due to the singularity of $\mathrm{d}\overline{P}_n^m(\varphi)/\mathrm{d}\varphi, \mathrm{d}^2\overline{P}_n^m(\varphi)/\mathrm{d}\varphi^2$ and $\mathrm{d}^3\overline{P}_n^m(\varphi)/\mathrm{d}\varphi^3$ when computed by the recursion formulae at $\varphi = \pm\pi/2$, and partly a consequence of the application of the Jacobian matrix—through division by $\cos\varphi$, $\cos^2\varphi$ and $\cos^3\varphi$ terms therein—to obtain the physical from the natural components of the gradients. Note that resorting to the Laplace equation is a means for overcoming the singularity affecting, e.g., the component $V^*_{\lambda\lambda}$ of the second-order gradient, provided that a non-singular algorithm for computing the derivatives of the fnALFs is adopted, so that $V^*_{\varphi\varphi}$ is non-singular itself. The relative precision of *CLENSHAW* and *LEGENDRE* near the geographic poles has been evaluated by executing the two codes on GRID3 (see Table 15), a portion of a meridian circle at 250 km altitude, $-107°$ longitude and latitude varying from 86° ($\simeq$ 400 km from the pole) to 89.95° ($\simeq$ 5 km from the pole) at steps of 0.05°. In this way, the precision loss that characterizes the transition from the non-singular to the singular pattern has been examined. Figure 8 superimposes the internal comparisons of the two codes for the relevant gravity gradient components, i.e., those which involve derivatives of the fnALFs and/or division by some power of $\cos\varphi$. We observe that in the computation of the first- and second-order gradients, *LEGENDRE* and *CLENSHAW* exhibit approximately the same trend, with precision losses of four digits for the first-order gradient (V^*_φ) and up to seven digits for the second-order gradient ($V^*_{\lambda\varphi}$). Most of the third-order gravity gradient elements are characterized by a decrease from 14–15 to eight or six digits precision as the pole is approached (the only exceptions being $V^*_{\varphi\varphi r}$ and $V^*_{\lambda\lambda r}$), but in some cases the two curves are not overlapped throughout the latitude range considered: in the case of $V^*_{\varphi\varphi\varphi}$ and $V^*_{\varphi\varphi\lambda}$ *CLENSHAW* suffers a precision loss four digits greater than *LEGENDRE*.

From Fig. 8 it is also possible to estimate the size (radius) of the polar region where *LEGENDRE**8 and *CLENSHAW**8 provide the "singular" components of the gravity gradients with a precision level lower than an assumed minimum threshold of, e.g., 12 significant digits. Such radius can be approximately set at 2° for all the gravity gradient components, except for $V^*_{\lambda\lambda\lambda}$, $V^*_{\varphi\varphi\lambda}$, $V^*_{rr\lambda}$ and $V^*_{\lambda\varphi r}$, for which the low-precision regime covers larger distances (i.e., 3°–4°) from the pole. Inside the low-precision regions, either resorting to non-singular algorithms or switching to quadruple precision is advisable. Furthermore, it has to be noted that Eqs. (10), (12) and (13) explicitly depend on various powers of n and m, and hence on the maximal degree N, which therefore influences the accuracy loss as a function of latitude.

Following Holmes and Featherstone (2002a), the internal tests have been supplemented with cross-comparisons among the four codes ("external comparisons"). For the external comparisons, the gravity gradient components computed with *PINES* and *METRIS* (global coordinates) have been rotated (see, e.g., Casotto and Fantino 2008) to the reference frame in which the output of *LEGENDRE* and *CLENSHAW* is given (i.e., local coordinates). The external comparisons presented here are based on the adoption of *CLENSHAW* in quadruple floating point precision (*CLENSHAW**16) as the reference code for assessing the numerical precision of the other three in double and quadruple precision modes. Table 1

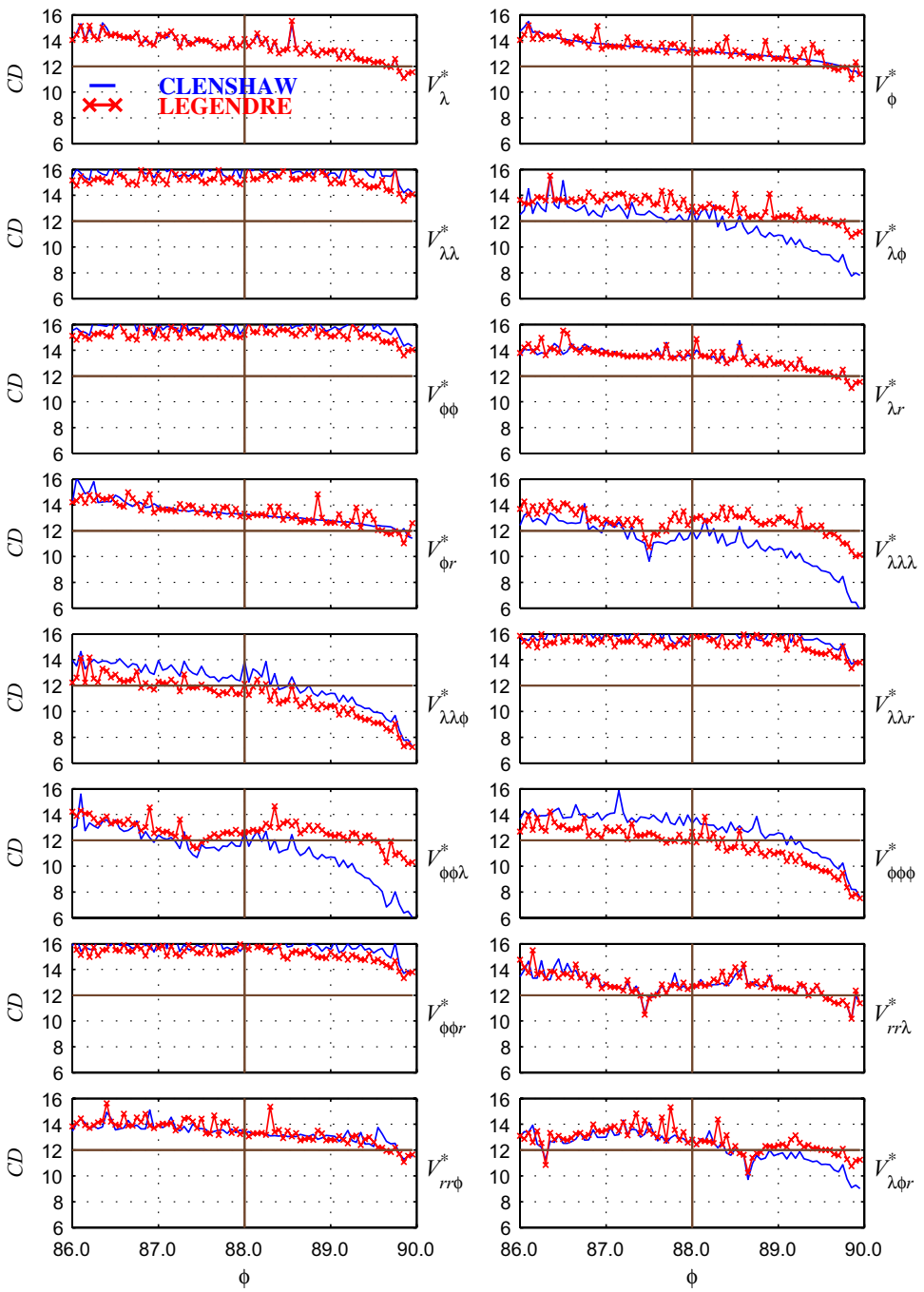

Fig. 8 Internal comparisons close to the North geographic pole for the relevant components of the first three gradients: the relative numerical precision of the double versus the quadruple versions of the two singular codes (i.e., *CLENSHAW* and *LEGENDRE*) is given as a function of latitude (from 86° to 89.95°, see the specifications of GRID3 in Table 15). Two solid lines (one horizontal and one vertical have been drawn to approximately indicate the geographical region around the pole ($\varphi \geq 88°$) where the relative numerical precision curves of *LEGENDRE**8 and *CLENSHAW**8 get below an assumed minimum precision level of 12 significant digits

of the ESM provides the global averages (over the grid) of the number of common significant digits between the gravity gradient components of each combination of software codes: the agreement between *CLENSHAW* and *LEGENDRE* is very good, with averages between 13 and 15 digits for *LEGENDRE**8 and above 32 for *LEGENDRE**16. The numerical precision relative to *CLENSHAW* gets worse when turning to *PINES* (12–15 and 30–32, respectively for the double and the quadruple precision modes) and then to *METRIS* (10–15 and 30–32).

However, it has to be noted that the coordinate transformation applied to the results of *PINES* and *METRIS* have some, although random, deteriorating effect on the data: possible causes are the additional numerical error introduced by the computation of the trigonometric functions of λ and φ, and the numerical error brought by individual gravity gradient elements when they combine to give one rotated component. The numerical comparison between *PINES* and *METRIS* before and after transforming from global to local coordinates is reported in Table 2 of the ESM: an average

numerical agreement always above 32 decimal places in global coordinates turns into a spread of values ranging between 30 and 33 in local coordinates.

Table 3 of the ESM lists the units and magnitude ranges of the local averages of each gravity gradient component in local coordinates over a geocentric sphere at 250 km height from the Earth's surface. Digital colour maps of the geopotential and its first-, second- and third-order gradients in the local reference frame are illustrated in Figs. 5–24 of the ESM.

7.3 Accuracy

The numerical accuracy of the four codes has been further verified by computing the values of certain analytical identities incorporating partial or final results of the gravity gradient synthesis. The most important and well-known of these is the Laplace equation:

$$\sum_{i=1}^{3} V_{ii}^{*} = 0. \tag{105}$$

Since the Laplacian is identically zero in empty space, the following sums are also zero:

$$\sum_{i=1}^{3} V_{iik}^{*} = 0, \quad k = 1, 2, 3. \tag{106}$$

Other exact relations that can be employed to check the accuracy are finite sums of the fnALFs and their derivatives, when such quantities are available. Three of these can be found for example in Holmes and Featherstone (2002a,b):

$$\sum_{n=0}^{N}\sum_{m=0}^{n}\left(\overline{P}_n^m(\varphi)\right)^2 = (N+1)^2, \tag{107}$$

$$\sum_{n=0}^{N}\sum_{m=0}^{n}\left(\frac{d\overline{P}_n^m(\varphi)}{d\varphi}\right)^2 = \frac{N(N+2)(N+1)^2}{4}, \tag{108}$$

and

$$\sum_{n=0}^{N}\sum_{m=0}^{n}\left(\frac{\mathrm{d}^2\overline{P}_n^m(\varphi)}{d\varphi^2}\right)^2 = N(N+2)(N+1)^2 \times \frac{(N+1)^2-2}{8}. \tag{109}$$

A fourth relation holds for the third-order derivatives of the fnALFs. It can be obtained, like the ones above, using the derivatives of the ALFs summation formula given by Winch and Roberts (1995):

$$\sum_{n=0}^{N}\sum_{m=0}^{n}\left(\frac{\mathrm{d}^3\overline{P}_n^m(\varphi)}{d\varphi^3}\right)^2 = N(N+2)(N+1)^2 \times \frac{16+5N(N+3)(N+2)(N-1)}{64}. \tag{110}$$

The numerical accuracy has been verified by evaluating Eqs. (105) and (106) with each of the four codes in GRID2 mode (see Table 15), whereas Eqs. (107)–(110) have been numerically verified on GRID2 only with *LEGENDRE* because the other three codes do not compute ALFs (except for the sectorial terms and their derivatives in the *Clenshaw* method). No rotations have been applied in this case: all identities have been computed in the native reference frame of the each individual code.

The grid average $\langle Id \rangle$ for each identity is defined as

$$\langle \mathrm{Id} \rangle = \left(\sum_{k=1}^{N_{\mathrm{obs}}} \mathrm{Id}^{(k)}\right) \Big/ N_{\mathrm{obs}}, \tag{111}$$

where Id denotes any of Eqs. (105)–(110), N_{obs} is the number of grid points and the superscript k refers to the k^{th} grid point. The results of the computations carried out with the different codes are shown in Table 18 for Eqs. (105)–(106) and in Table 19 for the specific cases of Eqs. (107)–(110). The Laplace identity is verified on average always at the level of $10^{-22}/10^{-21}$ in double precision and 10^{-39} in quadruple precision.

For the four identities involving partial sums of fnALFs and their derivatives [i.e., Eqs. (107)–(110)], the average is at the level of 10^{-14} and 10^{-32} in double and quadruple precision, respectively. It can be concluded that all four codes provide final (and partial) results characterized by very good numerical accuracy.

8 Summary and conclusions

This paper deals with the numerical comparison among four algorithms for harmonic synthesis applied to the computation of the geopotential and its first-, second- and third-order gradients: the traditional *Legendre* algorithm and its rearrangement following the Clenshaw formula, both based on the standard IDR on fnALFs; the *Pines* method based upon the direction cosines and the geocentric distance of the observation point and consisting in the same IDR recursion applied to fnHPs; the algorithm of *Cunningham–Metris* in global Cartesian coordinates involving IDR on solid spherical harmonics. To all four algorithms the lumped coefficients approach has been applied, which in most cases has implied a complete rearrangement of the equations forming the theory, as can be seen by inspection of Tables 1, 2, 3, 4, 5, 6, 7, and 8 and comparison with the original algorithms (especially PN73 and MT99). Furthermore, with respect to the algorithm published by PN73, the *Pines* method described and implemented here is based on the more stable IDR recursion formula for the computation of the Helmholtz polynomials, and its formulation has been extended to the third-order gradients of the geopotential. The computation of the third-order

Table 18 Grid average values for the Laplacian (Eq. 105) and the three identities of Eq. (106) as obtained with the four codes over GRID2 according to Eqs. (111)

Two levels of machine precision (REAL*8 and REAL*16) have been considered

Identity	Precision	*CLENSHAW*	*LEGENDRE*	*PINES*	*METRIS*
Equation (105)	REAL*8	-0.324×10^{-22}	-0.140×10^{-21}	-0.141×10^{-21}	-0.241×10^{-21}
	REAL*16	-0.117×10^{-39}	-0.438×10^{-39}	-0.363×10^{-39}	-0.102×10^{-39}
Equation (106)	REAL*8	-0.217×10^{-31}	0.152×10^{-31}	-0.376×10^{-29}	0.677×10^{-29}
$k = 1$	REAL*16	0.226×10^{-49}	0.652×10^{-50}	0.335×10^{-46}	-0.111×10^{-46}
Equation (106)	REAL*8	-0.926×10^{-31}	-0.830×10^{-30}	-0.351×10^{-29}	-0.698×10^{-28}
$k = 2$	REAL*16	-0.216×10^{-49}	-0.362×10^{-48}	-0.182×10^{-46}	0.103×10^{-46}
Equation (106)	REAL*8	-0.737×10^{-28}	-0.497×10^{-28}	-0.424×10^{-28}	-0.140×10^{-27}
$k = 3$	REAL*16	-0.116×10^{-46}	-0.300×10^{-46}	-0.443×10^{-46}	0.235×10^{-46}

Table 19 Grid averages of the four identities of Eqs. (107)–(110) as computed with *LEGENDRE* on GRID2 according to Eq. (111)

Identity	Precision average value		Exact value
Equation (107)	REAL * 8	$0.1303209999999995 \times 10^{6}$	0.130321×10^{6}
	REAL * 16	$0.13032100000000000000000000000073 \times 10^{6}$	
Equation (108)	REAL * 8	$0.4245858179999987 \times 10^{10}$	$0.424585818 \times 10^{10}$
	REAL * 16	$0.42458581800000000000000000000209 \times 10^{10}$	
Equation (109)	REAL * 8	$0.2766579960797095 \times 10^{15}$	$0.27665799607971 \times 10^{15}$
	REAL * 16	$0.27665799607971000000000000000128 \times 10^{15}$	
Equation (110)	REAL * 8	$0.2253344795978943 \times 10^{20}$	$0.2253344795978947668 \times 10^{20}$
	REAL * 16	$0.22533447959789476680000000000103 \times 10^{20}$	

The exact values of the corresponding identities for $N = 360$ are shown in the last column. Two levels of machine precision (REAL*8 and REAL*16) have been considered

gradient has been carried out also for the *Legendre* and *Clenshaw* methods, which in the geodetic literature are limited to the second order, whereas *Cunningham–Metris* is intrinsically applicable to gradients of arbitrary order.

The four algorithms have been implemented in dedicated software codes. For the *Cunningham–Metris* algorithm, the MT99 code has been used to provide the routines for the core computations, whereas code architecture, programming language, memory usage, and the machine precision have been entirely changed.

The four codes have been tested on the full EGM96 geopotential model on a GOCE-like orbit and several regular, spherical grids at satellite altitude. The performance tests, although with important precautions concerning compiler optimization and memory access, suggest a general agreement among the four codes on grid-type simulations. On the orbit, the tests indicate low performance levels for *METRIS* relative to the others: the most likely explanation is the less efficient data storage and, therefore, the slower memory access. This suggests that further improvements in the arrangement of the data structures of *METRIS* may produce better performances. In general, it can be concluded that thanks to the lumped coefficients approach, improved architecture and better memory handling, the new codes outperform those referenced in Casotto and Fantino (2007).

The accuracy tests confirm the capability of the four codes to accurately reproduce known identities both in double and quadruple machine precision. All four codes perform well in terms of relative precision, as shown by comparing the double with the quadruple precision versions of each code, although the overall numerical precision levels of *CLENSHAW* and *LEGENDRE* are generally better than those of the other two codes. *PINES* and *METRIS* are affected by an intrinsic loss of precision at the equator and suffer from additional deterioration when the gravity gradients components are rotated to the East-North-Up topocentric reference system. *CLENSHAW* and *LEGENDRE* suffer from singularities at the geographic poles as far as the geopotential gradients are concerned, partly inherent in the algorithm for computing the derivatives of the fnALFs, and partly due to the division by various powers of the cosine of the latitude when applying the Jacobian transformation from natural to physical components. For several gravity gradient components, a high-resolution analysis shows an increasing precision degradation, ranging from a loss of three significant digits at 2° from the geographic poles all the way to singularity at $\varphi = \pm 90°$.

It can be concluded that the algorithms discussed in this work are well suited to the purpose of accurately computing the potential and its first three gradients for gravitational fields ranging up to degree and order 360, which is largely sufficient for current orbital and space-geodetic applications. The several issues that have been addressed when presenting the algorithms and discussing the results of the tests should, however, be kept in mind when selecting a gravity gradient synthesis method for application to a specific problem.

Acknowledgments This research was supported by the Italian Space Agency (ASI). This support is gratefully acknowledged. The authors highly appreciate the valuable comments and critical remarks of C. C. Tscherning, S. Holmes, W. E. Featherstone and N. Sneeuw. E. F. also thanks M. Bardella and F. Biscani for helpful discussions.

Appendix A

The algorithm developed by Clenshaw (1955) and known under the name of *Clenshaw summation* was originally introduced as a recursion method to evaluate summations of series of Chebyshev polynomials. In general, it is a method for computing sums of products between indexed coefficients and functions which obey a three-term recurrence relation.

By adopting an approach similar to that of Press et al. (1992), let us consider the finite series

$$v(x) = \sum_{n=0}^{N} c_n p_n(x), \tag{A1}$$

in which the c_n coefficients are known and the $p_n(x)$ functions satisfy the three-term recurrence relation

$$p_n(x) - \alpha_n(x) p_{n-1}(x) - \beta_n(x) p_{n-2}(x) = 0, \tag{A2}$$

$\alpha_n(x)$ and $\beta_n(x)$ being known functions of the variable x. For the sake of simplicity, in the following we neglect the dependence on x in all the involved quantities.

Let us define recursively the set of coefficients y_n ($n = 0, 1, \ldots, N, N+1, N+2$):

$$\begin{aligned} y_{N+2} &= y_{N+1} = 0 \\ y_n &= c_n + \alpha_{n+1} y_{n+1} + \beta_{n+2} y_{n+2}. \end{aligned} \tag{A3}$$

By expressing the c_n's as a function of the y_n's, Eq. (A1) becomes

$$\begin{aligned} v = {} & [y_0 - \alpha_1 y_1 - \beta_2 y_2]\, p_0 \\ & + [y_1 - \alpha_2 y_2 - \beta_3 y_3]\, p_1 \\ & + [y_2 - \alpha_3 y_3 - \beta_4 y_4]\, p_2 + \cdots \\ & + \left[y_n - \alpha_{n+1} y_{n+1} - \beta_{n+2} y_{n+2}\right] p_n + \cdots \\ & + \left[y_N - \alpha_{N+1} y_{N+1} - \beta_{N+2} y_{N+2}\right] p_N \end{aligned} \tag{A4}$$

$$\begin{aligned} = {} & y_0 p_0 \\ & + y_1 [p_1 - \alpha_1 p_0] \\ & + y_2 [p_2 - \alpha_2 p_1 - \beta_2 p_0] \\ & + y_3 [p_3 - \alpha_3 p_2 - \beta_3 p_1] + \cdots \\ & + y_n \left[p_n - \alpha_n p_{n-1} - \beta_n p_{n-2}\right] + \cdots \\ & + y_N \left[p_N - \alpha_N p_{N-1} - \beta_N p_{N-2}\right] \\ & - y_{N+1} \alpha_{N+1} p_N - y_{N+2} \beta_{N+2} p_N. \end{aligned} \tag{A5}$$

Finally, using Eq. (A2) and the first of Eqs. (A3), we conclude that

$$\begin{aligned} v = {} & y_0 p_0 + y_1 [p_1 - \alpha_1 p_0] \\ & + y_2 \cdot 0 + y_3 \cdot 0 + \cdots + y_n \cdot 0 + \cdots + y_N \cdot 0, \end{aligned} \tag{A6}$$

from which

$$v = y_0 p_0 + y_1 p_1 - \alpha_1 y_1 p_0, \tag{A7}$$

i.e., the summation Eq. (A1) reduces to the sum of three terms, bringing considerable computational savings. Besides, as observed by Tscherning (1976), the *Clenshaw summation* starts by summing the high-order terms, making the algorithm well suited for most geodetic applications where the higher-order terms are in general small with respect to the lower-order ones.

References

Abramowitz M, Stegun IA (1964) Handbook of mathematical functions with formulas, graphs, and mathematical tables. Dover Publications, New York

Albertella A, Migliaccio F, Sansò F, Tscherning CC (2000) The space-wise approach—overall scientific data strategy. In: Sünkel H (ed) From Eötvös to mGal, Final Report, ESA/ESTEC contract No. 13392/98/NL/GD, GOCE Study Report. http://esamultimedia.esa.int/docs/Eoetvoes2Mgal_FinalReport_13392_98.pdf

Albertella A, Migliaccio F, Sansò F (2002) GOCE: the earth gravity field by space gradiometry. Celestial Mech Dyn Astron 83:1–15

Arsov K, Pail R (2003) Assessment of two methods for gravity field recovery from GOCE GPS-SST orbit solutions. Adv Geosci 1:121–126

Balmino G, Barriot J-P, Valès N (1990) Non-singular formulation of the gravity vector and gravity gradient tensor in spherical harmonics. Manuscr Geod 15(1):11–16

Balmino G, Barriot J-P, Koop R, Middel B, Thong NC, Vermeer M (1991) Simulation of gravity gradients: a comparison study. Bull Géod 65(4):218–229

Bettadpur SV, Schutz BE, Lundberg JB (1992) Spherical harmonic synthesis and least squares computations in satellite gravity gradiometry. Bull Géod 66(3):261–271

Casotto S, Fantino E (2007) Evaluation of methods for spherical harmonic synthesis of the gravitational potential and its gradients. Adv Sp Res 40:69–75

Casotto S, Fantino E (2008) Gravitational gradients by tensor analysis with application to spherical coordinates. J Geod. doi:10.1007/s00190-008-0276-z

Clenshaw CW (1955) A note on the summation of Chebyshev series. Math Tab Automat Comput 9:118–120

Cunningham LE (1970) On the computation of the spherical harmonic terms needed during the numerical integration of the orbital motion of an artificial satellite. Celestial Mech 2:207–216

Deprit A (1979) Note on the summation of Legendre Series. Celestial Mech 2:319–323

Drinkwater MR, Floberghagen R, Haagmans R, Muzi D, Popescu A (2003) GOCE: ESA's first earth explorer core mission. In: Beutler GB, Drinkwater M, Rummel R, von Steiger R (eds) Earth gravity field from space—from sensors to earth sciences. Space Sciences Series of ISSI, vol 18. Kluwer, Dordrecht, pp 419–432

Eddy WF, McCarthy JJ, Pavlis DE, Marshall JA, Luthcke SB, Tsaussi LS, Leung G, Williams DA (1990) GEODYN II—systems description, vol 1. STX Systems Corp., prepared for NASA/GSFC Space Geodesy Branch, Greenbelt

Ellis TMR, Philips IR, Lahey TM (1994) FORTRAN 90 programming. Addison-Wesley, England

ESA (1999) Gravity field and steady-state ocean circulation mission, ESA SP-1233(1). Report for mission selection of the four candidate earth explorer missions. http://www.esa.int/esaLP/GTCVCKSC_LPgoce_0.html

Garmier R, Barriot J-P (2001) Ellipsoidal harmonic expansions of the gravitational potential: theory and application. Celestial Mech Dyn Astron 79:235–275

Gautschi W (1967) Computational aspects of three-term recurrence relations. SIAM Rev 9(1):24–82

Gill E, Montenbruck O, Terzibaschian Th (2000) An Autonomous Navigation System for the German Small satellite Mission BIRD. Paper AAS 00-122

Gottlieb RG (1993) Fast gravity, gravity partials, normalized gravity, gravity gradient torque and magnetic field: derivation, code and data, NASA Contractor Report No. 188243

Heiskanen WA, Moritz H (1967) Physical geodesy. Freeman, San Francisco

Hobson EW (1965) The theory of spherical and ellipsoidal harmonics. Chelsea Publishing Company, New York

Holmes SA, Featherstone WE (2002a) A unified approach to the Clenshaw summation and the recursive computation of very high degree and order normalized associated Legendre functions. J Geod 76:279–299

Holmes SA, Featherstone WE (2002b) SHORT NOTE: extending simplified high-degree synthesis methods to second latitudinal derivatives of geopotential. J Geod 76:447–450

Ilk KH (1983) Ein Beitrag zur Dynamik ausgedehnter Körper—Gravitationswechselwirkung. PhD Thesis, Bayerischen Akademie der Wissenschaften, Munchen

Jackson MJ, Pollack HN, Sutton ST (1991) On the distribution of anomalous mass within the earth: forward models of the gravitational potential spectrum using ensembles of discrete mass elements. Geophys J Int 107:83–94

Jekeli C, Lee JK, Kwon HJ (2007) On the computation and approximation of ultra-high degree spherical harmonics. J Geod 81:603–615

Junkins JL (1976) An Investigation of Finite Element Representations of the Geopotential. AIAA J 14(6):803–808

Junkins JL, Engels RS (1979) The finite element approach in gravity modeling. Manuscr Geod 4:185–206

Keller W, Sharifi MA (2005) Satellite gradiometry using a satellite pair. J Geod 78:544–557

Konopliv AS, Binder AB, Hood LL, Kucinskas AB, Sjogren WL, Williams JG (1998) Improved gravity field of the moon from Lunar prospector. Science 281:1476–1480

Koop R, Stelpstra D (1989) On the computation of the gravitational potential and its first and second order derivatives. Manuscr Geod 14:373–382

Koop R (1993) Global gravity field modeling using satellite gravity gradiometry, The Netherlands Geodetic Comission, Publications on Geodesy, New Series, No. 38, Delft, The Netherlands

Koop R, Visser P, van den Ijssel J, Klees R (2000) Detailed scientific Data Processing Approach. In: Sünkel H (ed) From Eötvös to mGal, Final Report, ESA/ESTEC contract No. 13392/98/NL/GD, GOCE Study Report. Online version at http://esamultimedia.esa.int/docs/Eoetvoes2Mgal_FinalReport_13392_98.pdf

Lemoine FG, Kenyon SC, Factor JK, Trimmer RG, Pavlis NK, Chinn DS, Cox CM, Klosko SM, Luthcke SB, Torrence MH, Wang YM, Williamson RG, Pavlis EC, Rapp RH, Olson TR (1998) The Development of the Joint NASA GSFC and NIMA Geopotential Model EGM96. NASA/TP-1998-206861, NASA Goddard Space Flight Center

Long AC, Cappellari JO, Velez CE, Fuchs AJ (eds) (1989) Goddard trajectory determination system (GTDR), Mathematical Theory (Revision 1). NASA/GSFC Report FDD/552-89/0001, Greenbelt

Lundberg JB, Schutz BE (1988) Recursion formulas for Legendre functions for use with nonsingular geopotential models. J Guidance Control Dyn 11(1):31–38

McCarthy DD, Petit G (2004) IERS conventions (2003) (IERS Technical Note No. 32). BKG, Frankfurt am Main. Online version at http://www.iers.org/iers/publications/tn/tn32/

Metris G, Xu J, Wytrzyszczak I (1999) Derivatives of the gravity potential with respect to rectangular coordinates. Celestial Mech Dyn Astron 71:137–151. http://wwwrc.obs-azur.fr/cerga/mecanique/potential/

Michelson I (1970) Simplified analysis of mascon modification of Apollo-type orbits. Pure Appl Geophys 79:5–13

Migliaccio F, Reguzzoni M, Sansò F, Tscherning CC (2004) An Enhanced Space-Wise Simulation for GOCE Data Reduction. In: Proceedings of the second international GOCE user workshop (ESA SP-569)

Migliaccio F, Reguzzoni M, Sansò F, Tselfes N, Tscherning CC, Veicherts M (2006) The latest test of the space-wise approach for GOCE data analysis. In: Proceedings of the third international GOCE user workshop (ESA SP-627)

Montenbruck O, Gill E (2000) Satellite orbits—models, methods, and applications. Springer, Berlin

Pail R, Schuh WD, Wermuth M (2005) GOCE gravity field processing. In: Jekeli C, Bastos L, Fernandes J (eds) Gravity, Geoid and Space Missions International Association of Geodesy Symposia, vol 129. Springer, Berlin, pp 36–41

Pail R, Metzler B, Preimesberger T, Lackner B, Wermuth M (2006) GOCE quick-look gravity field analysis in the framework of HPF, in Proceedings of the Third International GOCE User Workshop (ESA SP-627)

Pavlis NK, Holmes SA, Kenyon SC, Schmidt D, Trimmer R (2005) A Preliminary Gravitational Model to Degree 2160. In: Jekeli C, Bastos L, Fernandes J (eds) "Gravity, Geoid and Space Missions" International Association of Geodesy Symposia, vol 129. Springer, Berlin, pp 18–23

Pines S (1973) Uniform representation of the gravitational potential and its derivatives. AIAA J 11:1508–1511

Press WH, Teukolsky SA, Vetterling WT, Flannery BP (1992) Numerical Recipes in Fortran 77. Cambridge University Press, Cambridge

Robin L (1957) Fonctions Sphériques de Legendre et Fonctions Sphéroidales—Tome I. Gauthier, Villars, Paris

Reguzzoni M (2003) From the time-wise to space-wise GOCE observables. Adv Geosci 1:137–142

Rummel R, Colombo OL (1985) Gravity field determination from satellite gradiometry. Bull Géod 59(3):233–246

Rummel R, Van Gelderen M, Koop R, Schrama E, Sansò F, Brovelli M, Migliaccio F, Sacerdote F (1993) Spherical harmonic analysis of satellite gradiometry. Publications on Geodesy, New Series, No. 39, Netherlands Geodetic Commission

Sansone G (1991) Orthogonal functions. Dover Publications, New York

Smoktunowicz A (2002) Backward stability of Clenshaw's algorithm. BIT Numer Math 42:600–610

Sneeuw N (2000) A semi-analytical approach to gravity field analysis from satellite observations. Deutsche Geodätische Kommission, Reihe C, Heft Nr. 527, München

Spencer JL (1976) Pines' nonsingular gravitational potential derivation, description and implementation. Technical report, NASA Contract No. 9-13970

Sutton ST, Pollack HN, Jackson MJ (1991) Spherical harmonic representation of the gravitational potential of spherical mass elements. Geophys J Int 107:77–82

Thông NC, Grafarend EW (1989) A spheroidal harmonic model of the terrestrial gravitational field. Manuscr Geod 14:285–304

Tóth Gy (2005) The gradiometric-geodynamic boundary value problem. In: Jekeli C, Bastos L, Fernandes J (eds) "Gravity, Geoid and Space Missions" International Association of Geodesy Symposia. vol 129. Springer, Berlin, pp 352–257

Tóth Gy, Földváry L (2005) Effect of geopotential model errors on the projection of GOCE gradiometer observables. In: Jekeli C, Bastos L, Fernandes J (eds) "Gravity, Geoid and Space Missions" International Association of Geodesy Symposia, vol 129. Springer, Berlin, pp 72–76

Tscherning CC (1976) Computation of the second-order derivatives of the normal potential based on the representation by a Legendre series. Manuscr Geod 1:71–92

Tscherning CC, Poder K (1982) Some geodetic applications of Clenshaw summation. Boll Geod Sci Aff XLI/4: 349–375

Tscherning CC, Rapp RH, Goad C (1983) A comparison of methods for computing gravimetric quantities from high degree spherical harmonic expansions. Manuscr Geod 8:249–272

Vallado DA (2001) Fundamentals of astrodynamics and applications. Microcosm Press/Kluwer, El Segundo/Dordrecht

Vanicek P, Krakiwski EJ (1986) Geodesy: the concepts. Elsevier, Amsterdam

Winch DE, Roberts PH (1995) Derivativs of addition theorems for Legendre functions. J Austral Math Soc Ser B 37:212–234

Xu G (2003) GPS theory, algorithms and applications. Springer, Heidelberg